Contributions of the four essential entry glycoproteins to HSV-1 tropism and the selection of entry routes.

Adam T. Hilterbrand[a], Raecliffe E. Daly[a,b], Ekaterina E. Heldwein[a,b,#]

[a]Department of Molecular Biology and Microbiology, Tufts University School of Medicine, Boston, MA 02111

[b]Graduate Program in Cellular, Molecular, and Developmental Biology, Tufts University School of Medicine, Boston, MA 02111

Running Head: The use of pseudotypes for investigating HSV-1 entry

Keywords: Herpes simplex viruses, HSV-1, cell entry, endocytosis, inhibitors, pseudotypes

#Address correspondence to Ekaterina E. Heldwein, katya.heldwein@tufts.edu

Abstract

Herpes Simplex viruses (HSV-1 and HSV-2) encode up to 16 envelope proteins, four of which are essential for entry. However, whether these four proteins alone are sufficient to dictate the broad cellular tropism of HSV-1 and the selection of different cell-type dependent entry routes is unknown. To begin addressing this, we previously pseudotyped VSV, lacking its native glycoprotein G, with only the four essential entry glycoproteins of HSV-1: gB, gH, gL, and gD. This novel VSVΔG-BHLD pseudotype recapitulated several important features of HSV-1 entry: the requirement for gB, gH, gL, gD, a cellular receptor, and sensitivity to anti-gB and anti-gH/gL neutralizing antibodies. However, due to the use of a single cell type in that study, the tropism of the VSVΔG-BHLD pseudotype was not investigated. Here, we show that the cellular tropism of the pseudotype is severely limited compared to wild-type HSV-1 and that its entry pathways differ from the native HSV-1 entry pathways. To test the hypothesis that other HSV-1 envelope proteins may contribute to HSV-1 tropism, we generated a derivative pseudotype containing the HSV-1 glycoprotein gC (VSVΔG-BHLD-gC) and observed a gC-dependent increase in entry efficiency in two cell types. We propose that the pseudotyping platform developed here has the potential to uncover functional contributions of HSV-1 envelope proteins to entry in a gain-of-function manner.

Importance

Herpes simplex viruses (HSV-1 and HSV-2) contain up to 16 different proteins in their envelopes. Four of these, glycoproteins gB, gD, gH, and gL, are termed essential with regard to entry whereas the rest are typically referred to as non-essential based on the entry phenotypes of the respective single genetic deletions. However, the single-gene deletion approach, which relies

40 on robust loss-of-function phenotypes, may be confounded by functional redundancies among
41 the many HSV-1 envelope proteins. We have developed a pseudotyping platform, in which the
42 essential four entry glycoproteins are isolated from the rest, which can be added back
43 individually for systematic gain-of-function entry experiments. Here, we show the utility of this
44 platform for dissecting the contributions of HSV envelope proteins, both the essential four and
45 the remaining dozen (using gC as an example), to HSV entry.
46

47 **Introduction**

48 Herpes simplex viruses (HSV-1 and HSV-2) are enveloped viruses that infect much of the
49 world's population for life and cause diseases ranging from painful oral or genital lesions to
50 serious conditions such as encephalitis and blindness (1, 2). These viruses enter target cells by
51 different, cell-type specific routes. For example, they enter neurons by direct fusion of their
52 envelopes with the plasma membrane (3) and epithelial cells by endocytosis followed by fusion
53 with an endosomal membrane (4, 5). While these entry pathways have been broadly described,
54 the underlying mechanisms and the contributions of individual viral and cellular proteins to the
55 selection of these entry routes remain incomplete.

56 HSV-1 entry by any route requires the coordinated efforts of four glycoproteins – gB, gH,
57 gL, and gD, which are essential for entry (6-8) – and a cellular gD receptor (3, 9, 10). gB, gH,
58 gL, and gD are also sufficient for cell-cell fusion of uninfected receptor-bearing cells expressing
59 these four glycoproteins (11, 12). The prevalent model, which was largely developed through
60 studies using the cell-cell fusion system, posits that these four viral glycoproteins orchestrate
61 membrane fusion through a sequential activation process termed a cascade (13, 14). First, gD
62 binds one of its three cellular receptors, nectin-1, herpesvirus entry mediator (HVEM), or 3-O-

63 sulfated heparan sulfate (3-OS-HS) (15). Binding of gD to its receptor triggers a conformational
64 change within gD (14, 16, 17) that enables it to bind (18) and activate the gH/gL heterodimer
65 (13, 19, 20). In turn, gH/gL presumably interacts with and activates gB (13, 21, 22), the fusogen
66 that mediates the merger of the HSV lipid envelope with the cellular membrane (9, 10, 14, 23).
67 In addition to the essential four glycoproteins, HSV-1 encodes up to 12 more envelope
68 proteins, eight glycosylated and four unglycosylated (24-26). Current models of HSV-1 entry do
69 not account for the potential effects of these envelope proteins. Therefore, being able to
70 functionally uncouple the four essential glycoproteins – gB, gH, gL, and gD – from the rest is
71 fundamental for elucidating their contributions to HSV-1 cellular tropism and entry pathways.
72 One powerful system that enables such studies is the vesicular stomatitis virus (VSV)-
73 based pseudotype, in which the native VSV glycoprotein, G, is replaced with a viral envelope
74 protein of interest (27). The VSV pseudotyping system allows one to define entry mechanisms
75 conferred by a specific viral glycoprotein by effectively isolating it from its native viral context.
76 This platform has been used to elucidate the entry mechanisms of many viruses, notably those
77 that require BSL-3 or BSL-4 containment facilities, including SARS-CoV (28, 29), SARS-CoV-
78 2 (30), Ebola virus (31), Lassa virus (32, 33), Lujo virus (34), Hantavirus (35), Rift Valley fever
79 virus (36), or those that are difficult to culture, such as Hepatitis C virus (37) or Japanese
80 encephalitis virus (38). The use of VSV pseudotypes has been particularly useful in identifying
81 cellular receptors of many viruses (31-36).
82 To determine whether the essential four HSV-1 glycoproteins were sufficient for entry,
83 we previously generated VSV lacking its native glycoprotein G and pseudotyped with HSV-1
84 gB, gH, gL, and gD through *trans*-complementation (VSVΔG-BHLD) (39). The VSVΔG-BHLD
85 pseudotype efficiently entered C10 cells (B78 murine melanoma cells expressing HSV-1

86 receptor nectin-1), and its entry – like that of HSV-1 – required gB, gH, gL, gD, and a gD
87 receptor, and was inhibited by anti-gB and anti-gH/gL neutralizing antibodies (39). However,
88 this study left unknown whether the VSVΔG-BHLD pseudotype could enter any HSV-1
89 susceptible cell types or utilize native entry routes. Therefore, we sought to directly compare the
90 cellular tropism and the entry pathways of the VSVΔG-BHLD pseudotype and HSV-1 to
91 determine the extent by which these were conferred solely by the four essential glycoproteins.
92 Here, we expanded our studies to six additional HSV-1 susceptible cell lines. VSVΔG-
93 BHLD was only able to enter, with reasonable efficiency, two out of the seven HSV-1-
94 susceptible cell lines. Additionally, the VSVΔG-BHLD pseudotype entered both cell lines by
95 routes different from those used by HSV-1. Differences in tropism and routes of entry could not
96 be accounted for by either cell-surface receptor levels, their nature (nectin-1 vs. HVEM), the
97 relative amounts of gB, gH, gL, and gD, or virion morphology (VSV vs. HSV-1). Therefore, we
98 conclude that the four essential HSV-1 entry glycoproteins are insufficient for entry into any
99 HSV-1-susceptible cell and do not specify native entry routes. Our results raise an intriguing
100 possibility that HSV-1-specific components outside the essential four glycoproteins influence
101 HSV-1 entry. Indeed, when the HSV-1 glycoprotein gC was included in the VSVΔG-BHLD
102 pseudotype (VSVΔG-BHLD-gC), entry efficiency into CHO-HVEM and HaCaT cells increased,
103 suggesting a cell-type dependent gain-of-function conferred by gC. Therefore, we hypothesize
104 that the so-called non-essential HSV-1 envelope proteins, which are missing from the VSVΔG-
105 BHLD pseudotype, are important in specifying both HSV-1 tropism and its routes of cell entry.
106
107 **Results**

108 ***VSVΔG-BHLD pseudotypes enter a limited repertoire of HSV-1 susceptible cells.*** To determine
109 the tropism of the VSVΔG-BHLD pseudotype, we selected seven HSV-1-susceptible cell lines
110 (Fig. 1). The cell lines B78H1 and CHO-K1, which lack HSV-1 receptors served as negative
111 controls. HSV-1 efficiently infected all seven receptor-bearing cells but not the receptor-negative
112 cells (Fig. 1A). The VSVΔG-BHLD pseudotype efficiently infected C10 cells (Fig. 1B),
113 consistent with our previous report (39). The VSVΔG-BHLD pseudotype also infected CHO-
114 HVEM, CHO-nectin-1, and HaCaT cells, albeit with lower efficiency (Fig. 1B). Although
115 VSVΔG-BHLD entry into CHO-HVEM and CHO-nectin-1 cells was relatively inefficient, it was
116 clearly receptor-dependent (Fig. 1B). However, no measurable VSVΔG-BHLD entry was
117 observed in HeLa, Vero, or SH-SY5Y cells (Fig. 1B) even at MOI of 10 (Fig. S1A).
118 Two additional VSV pseudotypes were used as controls. VSVΔG-G is VSVΔG
119 pseudotyped *in trans* with native VSV glycoprotein G (39) . VSVΔG-PIV5 is VSVΔG
120 pseudotyped with entry glycoproteins HN and F from parainfluenza virus 5 (PIV5) (40). Both
121 controls infected all 9 tested cell lines, with varying efficiency (Figs. S1B and C), suggesting the
122 limited tropism of VSVΔG-BHLD could not be attributed to VSV morphology alone.
123
124 ***Cell-surface receptor levels do not correlate with differences in VSVΔG-BHLD cellular***
125 ***tropism.*** We first asked whether differences in cell surface levels of HSV-1 receptors could
126 account for VSVΔG-BHLD entry efficiency. Levels of HSV-1 gD receptors nectin-1 and HVEM
127 vary across cell lines, and susceptibility to HSV-1 infection generally correlates with surface
128 receptor levels (41). Surface levels of nectin-1 and HVEM were measured in all 9 cell lines by
129 flow cytometry (Figs. 1C and D). As expected, neither receptor was detected on the receptor-

130 negative cell lines B78H1 and CHO-K1 (Figs. 1C and D). C10 and HaCaT cells had the highest
131 levels of nectin-1, whereas intermediate levels of nectin-1 were detected on CHO-nectin-1,
132 HeLa, Vero and SH-SY5Y cells (Fig. 1C). CHO-HVEM cells had high levels of HVEM but no
133 detectable nectin-1 on their surface (Fig. 1D). In addition to nectin-1, we also detected HVEM on
134 the surface of HaCaT and Vero cells (Fig. 1D), but the low amounts of HVEM suggested that
135 nectin-1 likely functions as the primary receptor in these cells. Surprisingly, while both C10 and
136 HaCaT cells expressed high levels of nectin-1, the VSVΔG-BHLD pseudotype efficiently
137 entered only C10 cells. These results suggest that surface receptor levels alone do not explain the
138 varying entry efficiencies of the VSVΔG-BHLD pseudotype into the tested cell lines.
139
140 ***Differences in tropism of VSVΔG-BHLD and HSV-1 do not correlate with the relative***
141 ***gB:gH:gL:gD ratios.*** HSV-1 and VSV acquire their envelopes from different sources: Trans
142 Golgi Network (TGN) or endosomes for HSV-1 (42, 43) vs. the plasma membrane (PM) for
143 VSV (27). Different envelope origins could affect the gB:gH:gL:gD ratios on viral particles and,
144 possibly, influence entry efficiency. To test this hypothesis, purified HSV-1 and VSVΔG-BHLD
145 particles were analyzed for gB, gH, gL, and gD content by western blot (Fig. 1E), and relative
146 gB:gH:gL:gD ratios were determined by densitometry. In each virus, levels of gH, gL, and gD
147 were normalized to their respective gB levels. We found that the gB:gH:gL:gD ratios in HSV-1
148 (1:0.47:0.05:1.36) and VSVΔG-BHLD (1:0.57:0.12:1.31) virions were similar (Fig. 1F) and
149 unlikely to account for the observed differences in tropism.
150
151 ***Entry of both VSVΔG-BHLD and HSV-1 into C10 and CHO-HVEM cells occurs by***
152 ***endocytosis.*** HSV-1 can enter different cell types by fusion at the plasma membrane (Vero and

153 SH-SY5Y) (5, 44) or by endocytosis (C10, CHO-nectin-1, CHO-HVEM, HeLa, and HaCaT) (3,
154 5, 45, 46). To compare the entry routes of the VSVΔG-BHLD pseudotype and HSV-1, we chose
155 C10 and CHO-HVEM cells because the VSVΔG-BHLD pseudotype infected C10 (~50%) or
156 CHO-HVEM (~8%) cells to an appreciable extent and in a receptor-dependent manner (Fig. 1B).
157 We first treated cells with a hypertonic solution of sucrose, a broad inhibitor of endocytic
158 pathways (47, 48). Entry of both HSV-1 and VSVΔG-BHLD into C10 and CHO-HVEM cells
159 was inhibited by sucrose (Fig. 2A-D), implicating endocytosis. As a control, sucrose also
160 prevented the endocytic uptake of Alexa Fluor 488-labeled transferrin into both C10 and CHO-
161 HVEM cells (Fig. S2E). As expected, sucrose did not inhibit entry of VSVΔG-PIV5 into either
162 cell line (Figs. S2B and D) because PIV5 enters by fusion at the plasma membrane (40, 49).
163 VSV entry occurs by endocytosis (50-52), and, accordingly, sucrose blocked entry of VSVΔG-G
164 into C10 cells (Fig. S2A). Surprisingly, it did not block entry into CHO-HVEM cells (Fig. S2C),
165 suggesting that the inhibitory effect of hypertonic sucrose on VSV-G-dependent entry is cell-
166 type specific.
167
168 ***VSVΔG-BHLD entry requires dynamin but not clathrin whereas HSV-1 entry requires both.***
169 Having established that the VSVΔG-BHLD pseudotype entered cells by endocytosis, we next
170 sought to identify the entry routes and compare them to those of HSV-1 by using both chemical
171 and genetic means of inhibiting various endocytic uptake pathways.
172 First, we examined the role of clathrin-mediated endocytosis (CME), one of the most
173 well studied endocytic pathways hijacked by viruses for entry (53, 54). CME requires both
174 clathrin, to promote receptor-mediated endocytosis (55), and dynamin, a GTPase that mediates
175 scission of the endocytic vesicle (56). We chose three commonly used dynamin inhibitors:

176 Dynasore, Dyngo-4a, and myristyltrimethylammonium bromide (MiTMAB) (47, 57). For
177 clathrin inhibition, we chose Pitstop-2, which selectively blocks CME by preventing ligand
178 association with the clathrin terminal domain (47). Another CME inhibitor, chlorpromazine,
179 which prevents clathrin association with the plasma membrane (47), was also tested but found to
180 be toxic to both C10 and CHO-HVEM cells. Inhibitory activity of all four compounds was
181 ascertained by their ability to inhibit CME of transferrin (Figs. S3E and F).

182 HSV-1 entry into both C10 and CHO-HVEM cell lines was inhibited by all four
183 inhibitors (Figs. 3A and B) indicating that HSV-1 enters both cell lines by CME. Entry of the
184 VSVΔG-BHLD pseudotype into C10 and CHO-HVEM cells was sensitive to all dynamin
185 inhibitors (Figs. 3C and D). However, Pitstop-2 did not block VSVΔG-BHLD entry (Figs. 3C
186 and D), suggesting that CME was not involved in entry. Collectively, these observations
187 suggested that HSV-1 enters both C10 and CHO-HVEM cells by CME whereas VSVΔG-BHLD
188 pseudotypes utilize a dynamin-dependent, clathrin-independent entry route. These results were
189 the first indication of possible differences in entry routes of HSV-1 and VSVΔG-BHLD.

190 Entry of the control VSVΔG-G pseudotype into C10 cells was blocked by all three
191 dynamin inhibitors and the clathrin inhibitor (Fig. S3A), and its entry into CHO-HVEM cells
192 was blocked by Pitstop-2 (Fig. S3C) and by two of three dynamin inhibitors, Dynasore and
193 Dyngo-4a (Fig. S4C), strongly implicating CME as the entry route (52, 58). VSVΔG-PIV5 entry
194 into CHO-HVEM cells was not blocked by any of the four inhibitors (Fig. S3D) while its entry
195 into C10 cells was blocked only by one out of three dynamin inhibitors, Dyngo-4a (Fig. S3C),
196 consistent with the previous report of entry into other cell types by fusion at the plasma
197 membrane (40, 49).
198

199 ***Cholesterol is important for entry of both VSVΔG-BHLD and HSV-1.*** Our results suggested
200 that VSVΔG-BHLD did not use CME for entry into either C10 or CHO-HVEM cells,
201 implicating a clathrin-independent endocytic (CIE) route. Caveolin-dependent endocytosis is a
202 major CIE (59) that is hijacked by viruses such as SV40 or Japanese encephalitis virus (60, 61).
203 Caveolin-1 is cellular protein that, similarly to clathrin, promotes membrane curvature and
204 subsequent endocytosis through the formation of caveolae (62). Caveolin-dependent entry
205 requires plasma membrane cholesterol for proper caveolin-1 association with the membrane (62,
206 63).
207 Previous work has demonstrated that cellular cholesterol was important for HSV-1 entry
208 into C10 cells (64). Similarly, entry of both HSV-1 and VSVΔG-BHLD into C10 and CHO-
209 HVEM cells decreased when cholesterol was removed from cellular membranes using a
210 cholesterol-depleting agent, methyl-β-cyclodextrin (MβCD) (Figs. 4A-D). Efficiency of
211 cholesterol depletion was confirmed by the reduction of the cholesterol-dependent association of
212 cholera toxin subunit B (CTB) (65) with C10 and CHO-HVEM cells upon MβCD treatment
213 (Fig. S4E). Entry of VSVΔG-G was insensitive to cholesterol depletion (Figs. S4A and C), as
214 reported for other cell types (66, 67). In the case of VSVΔG-PIV5, only entry into C10 cells was
215 cholesterol-dependent (Fig. S4B) whereas the entry into CHO-HVEM cells was not (Fig. S4D),
216 suggesting that cholesterol is required for VSVΔG-PIV5 entry in a cell-type dependent manner.
217 Entry of neither HSV-1 nor VSVΔG-BHLD into CHO-HVEM cells was reduced by the
218 knockdown of caveolin-1 (Fig. 4E), similarly to the VSVΔG-G and VSVΔG-PIV5 control
219 viruses (Fig. S4F). Successful knockdown was verified by western blot (Fig. 4F). Surprisingly,
220 no caveolin-1 was detected in C10 cells (Fig. 4G). Caveolin-1 was detected in 3T12 cells

221 (murine fibroblasts), which ruled out species-dependent recognition of murine vs. hamster
222 caveolin-1, (Fig. 4G). Therefore, C10 cells appear to express no detectable caveolin-1. We
223 conclude that while cellular cholesterol is important for the entry of both HSV-1 and VSVΔG-
224 BHLD, neither virus utilizes caveolin-1-mediated endocytosis for entry into C10 and CHO-
225 HVEM cells.
226
227 ***HSV-1 and VSVΔG-BHLD do not enter C10 and CHO-HVEM cells by macropinocytosis, but***
228 ***NHE1 and Rac1 are important for optimal VSVΔG-BHLD entry.*** We next evaluated the
229 potential involvement of macropinocytosis, another CIE commonly used by viruses (68). We
230 selected three known inhibitors of macropinocytosis: cytochalasin D (CytoD), 5-(N-Ethyl-N-
231 isopropyl)amiloride (EIPA), and NSC23766 (47). CytoD is a potent inhibitor of actin
232 polymerization that disrupts filamentous actin (47). EIPA blocks macropinocytosis by blocking
233 Na^+/H^+ exchange proteins (NHE), which decreases the intracellular pH and inhibits small
234 GTPase function important for macropinocytosis (69). NSC23766 blocks macropinocytosis by
235 inhibiting the activity of the small GTPase Rac1 (70). Inhibitory activity of all three compounds
236 was confirmed by their ability to inhibit macropinocytosis of rhodamine-B-labeled 70-kDa
237 dextran (Fig. S7E).
238 HSV-1 entry into either C10 or CHO-HVEM cells was not appreciably inhibited by any
239 of the macropinocytosis inhibitors (Figs. 5A and C). By contrast, VSVΔG-BHLD entry into both
240 C10 and CHO-HVEM cells was reduced by NSC23766 and, to a lesser extent, EIPA but not by
241 cytochalasin D (Figs. 5B and D). While the inhibitory effect of NSC23766 and EIPA would
242 appear to implicate macropinocytosis as the route of VSVΔG-BHLD entry into C10 and CHO-
243 HVEM cells, the lack of actin involvement argues against it. This is because assembly of

244 filamentous actin is essential for the formation of membrane ruffles and subsequent uptake
245 during macropinocytosis (71). Actin polymerization is, thus, a major hallmark of
246 macropinocytosis (68). Accordingly, we did not observe any appreciable co-localization of
247 VSVΔG-BHLD virions with the 70-kDa rhodamine B labeled dextran, a fluid phase uptake
248 marker (Figs. S5 and S6). Collectively, these results suggest that neither VSVΔG-BHLD nor
249 HSV-1 utilize macropinocytosis for entry into C10 or CHO-HVEM cells. However, NHE and
250 Rac1 facilitate VSVΔG-BHLD entry into both cell lines, presumably, independently of their role
251 in macropinocytosis.
252 Although VSV enters cells by CME rather than macropinocytosis, it has been shown to
253 require filamentous actin to achieve full engulfment of the viral particle by the plasma membrane
254 during endocytosis, as observed in BSC-1 cells, an African green monkey epithelial cell line (58,
255 72). Indeed, VSVΔG-G entry into C10 cells was modestly reduced by cytochalasin D and EIPA
256 but not NSC23766 (Fig. S7A) whereas its entry into CHO-HVEM cells was somewhat reduced
257 by EIPA but not cytochalasin D or NSC23766 (Fig. S7C). The apparent lack of actin
258 involvement in VSVΔG-G entry into CHO-HVEM cells may represent a cell-type specific
259 phenomenon. VSVΔG-PIV5 entry was not blocked with any of the three inhibitors of
260 macropinocytosis, consistent with fusion at the plasma membrane, and was, in fact, increased in
261 the presence of EIPA in C10 cells (Fig. S7B).
262
263 ***HSV-1 and VSVΔG-BHLD differ in their requirements for Rab GTPases for entry.*** Endocytic
264 entry by many viruses requires small GTPases known as Rabs. Rab GTPases are important for
265 the formation of endosomal compartments in the cell (73). Different viruses penetrate endocytic
266 membranes at distinct endosomal maturation stages – for example, VSV fuses with membranes

267 of early endosomes whereas influenza A virus fuses with membranes of late endosomes (74) –
268 so, proper formation of these endosomal compartments is essential for viral entry. GTPases Rab5
269 and Rab7 are important for the maturation and formation of early endosomes and late
270 endosomes/multi-vesicular bodies (MVBs), respectively (75). Overexpression of dominant
271 negative (DN) forms of either Rab5 (Rab5DN) or Rab7 (Rab7DN) suppress early and late
272 endosome formation, respectively (76, 77).

273 To identify the endosomal compartment(s) required for HSV-1 or VSVΔG-BHLD entry,
274 C10 and CHO-HVEM cells were transfected with constructs encoding fluorescently tagged
275 Rab5DN or Rab7DN and then infected. The transfection efficiency was 40-50% in C10 cells and
276 30-40% in CHO-HVEM cells as measured by flow cytometry. To determine entry efficiency by
277 flow cytometry, viral entry was calculated by dividing the percent of infected and transfected
278 cells by the total number of transfected cells. Overexpression of either Rab5DN or Rab7DN had
279 no significant effect on HSV-1 entry into either cell line (Figs. 6A and E). These results in C10
280 and CHO-HVEM cells agree with recent work that indicates HSV-1 enters CHO-HVEM cells by
281 a non-canonical endocytic route, independent of Rab5 or Rab7 (78). VSVΔG-BHLD entry into
282 CHO-HVEM cells was also unaffected by either Rab5DN or Rab7DN (Fig. 6G). However,
283 VSVΔG-BHLD entry into C10 cells was reduced in the presence of Rab5DN and, to some
284 extent, Rab7DN (Fig. 6C). We hypothesize that HSV-1 entry into both cell lines and VSVΔG-
285 BHLD entry into CHO-HVEM cells either do not depend on the endosomal maturation or occurs
286 very early after internalization, prior to the formation of early endosomes. By contrast, VSVΔG-
287 BHLD likely enters C10 cells out of early endosomes. This observation marked the first instance
288 of a difference in VSVΔG-BHLD entry into C10 vs. CHO-HVEM cells.

289 As expected, entry of VSVΔG-G into both C10 and CHO-HVEM cells was reduced in
290 the presence of Rab5DN (Figs. S8A and E), in accordance with reports of VSV fusing with
291 membranes of early endosomes (52). VSVΔG-PIV5 entry into C10 cells was insensitive to
292 Rab5DN or Rab7DN (Fig. S8C). Although VSVΔG-PIV5 entry into CHO-HVEM cells was
293 reduced by Rab5DN and Rab7DN in a statistically significant manner, the differences were
294 relatively small (Fig. S8G). This suggested that Rab5DN and Rab7DN have a minimal effect on
295 VSVΔG-PIV5 entry as expected for a virus that fuses with the plasma membrane.
296 Another small GTPase, ADP-ribosylation factor 6 (Arf6), which is involved in regulating
297 vesicular trafficking (79), regulates the endocytic entry of HIV, Coxsackievirus, and Vaccinia
298 virus (80-82). To probe the role of Arf6 in entry, cells were treated with NAV-2729, which
299 blocks Arf6 interaction with guanine exchange factors (GEFs) thereby preventing its activation
300 (83). HSV-1 entry into both C10 and CHO-HVEM cells was inhibited by NAV-2729 (Figs. 6B
301 and F) whereas VSVΔG-BHLD entry was not (Figs. 6D and H), which suggests that only HSV-1
302 entry requires Arf6 activity.
303 VSVΔG-PIV5 entry was not inhibited by NAV-2729 in either C10 or CHO-HVEM cells
304 (Figs. S8D and H). However, VSVΔG-G entry was inhibited by NAV-2729 in both C10 and
305 CHO-HVEM cells, suggesting that Arf6 could be involved in VSV endocytosis (Figs S8B and
306 F). These results point to a previously unappreciated role of Arf6 in HSV-1 and VSV entry.
307
308 ***Entry of the VSVΔG-BHLD pseudotype requires endosomal acidification in a cell-dependent***
309 ***manner.*** To investigate the role of endosomal acidification in entry, we used three common
310 inhibitors, NH_4Cl, a weak base; monensin, a carboxylic ionophore; and bafilomycin A1 (BFLA),
311 an endosomal V-ATPase inhibitor. Each inhibitor effectively blocked endosomal acidification as

312 evidenced by decrease in Lysotracker fluorescence in inhibitor-treated cells (Fig. S9E). Entry of
313 VSVΔG-G, which requires low pH as a trigger for membrane fusion, was sensitive to all three
314 inhibitors in both cell lines (Figs. S9A and C). By contrast, VSVΔG-PIV5 entry, which occurs by
315 fusion at the plasma membrane, was insensitive to any of the inhibitors (Figs. S9B and D).
316 VSVΔG-BHLD entry into C10 cells was inhibited by all three endosomal acidification
317 inhibitors (Fig. 7B) and thus appears to require endosomal acidification. VSVΔG-BHLD entry
318 into CHO-HVEM cells was inhibited only by one out of three inhibitors, NH_4Cl (Fig. 7D) and
319 likely does not require endosomal acidification. Interestingly, HSV-1 entry into both C10 and
320 CHO-HVEM cells was inhibited by NH_4Cl and monensin but not by BFLA (Figs. 7A and C).
321 We hypothesize that the discrepancy in the inhibitory effects among the three inhibitors could
322 potentially be due to the distinct mechanisms by which BFLA, NH_4Cl, and monensin raise
323 endosomal pH.
324
325 ***Glycoprotein C (gC) increases entry efficiency into CHO-HVEM and HaCaT cells.*** The much
326 narrower tropism of VSVΔG-BHLD pseudotype relative to HSV-1 suggested that envelope
327 proteins outside the essential four may contribute to HSV-1 tropism and entry efficiency. To test
328 this hypothesis, we generated a VSV-pseudotype containing gC in addition to gB, gH, gL, and
329 gD (VSVΔG-BHLD-gC) (Fig. 8A). To generate the VSVΔG-BHLD-gC pseudotype at
330 sufficiently high titers suitable for entry experiments, the amount of gB plasmid transfected into
331 HEK293T cells was increased. The corresponding VSVΔG-BHLD-pCAGGS control was
332 generated similarly. For yet unclear reasons, VSVΔG-BHLD-pCAGGS entered CHO-nectin-1,
333 CHO-HVEM, and HaCaT cells (Fig. 8B) more efficiently than the VSVΔG-BHLD pseudotype

334 (Fig. 1A). Transfection of higher amounts of the gB plasmid could, in principle, lead to a higher
335 expression levels of gB in the cells and, consequently, higher incorporation into the virions.
336 More importantly, however, the VSVΔG-BHLD-gC pseudotype entered CHO-HVEM and
337 HaCaT cells with a significantly higher efficiency than the VSVΔG-BHLD-pCAGGS
338 pseudotype (Fig. 8B). These results suggest that gC can increase cell entry efficiency in a cell-
339 specific manner.
340

341 **Discussion**

342 Decades ago, glycoproteins gB, gH, gL, and gD were established as essential for HSV-1 entry
343 (6-8). These four glycoproteins are also sufficient for cell-cell fusion when co-expressed in
344 uninfected, receptor-bearing cells (11, 12). While these studies greatly increased our
345 understanding of the HSV-1 entry and fusion mechanisms, it was unclear whether these four
346 glycoproteins were sufficient to specify cellular tropism and the selection of entry routes, partly
347 due to the presence of up to 12 other envelope proteins. To begin addressing this, we generated a
348 VSV-based pseudotype containing HSV-1 gB, gH, gL, and gD. Being devoid of other HSV-1
349 proteins, the VSVΔG-BHLD pseudotype provides a bare-bones platform to identify
350 contributions of the core set of four essential glycoproteins to HSV-1 cellular tropism and the
351 selection of entry routes.

352 Previously, we showed that the VSVΔG-BHLD pseudotype efficiently entered C10 cells
353 and that its entry recapitulated several important features of HSV-1 entry into susceptible cells:
354 the requirement for gB, gH, gL, gD, and a gD receptor and sensitivity to anti-gB and anti-gH/gL
355 neutralizing antibodies (39). Here, we expanded this study to six additional HSV-1-susceptible
356 cell lines and made two key observations. First, we found that in addition to C10 cells, only

357 CHO-HVEM cells supported appreciable VSVΔG-BHLD entry. Second, VSVΔG-BHLD and
358 HSV-1 entered these two cell lines by distinct endocytic mechanisms as judged by the
359 differences in sensitivity to various inhibitors (Fig. 9 and Table S1). These results imply that
360 alone, gB, gH, gL, and gD permit entry of VSV pseudotypes only into a limited range of HSV-1-
361 susceptible cell types and even then, do not specify native entry routes. On the basis of these
362 results, we hypothesize that other HSV-1 envelope proteins may have underappreciated roles in
363 defining HSV-1 tropism, entry route selection, or both. Although it may be too early to conclude
364 that the incorporation of gC into the VSVΔG-BHLD pseudotype has changed its tropism, the
365 increase in cell-specific entry efficiency of the VSVΔG-BHLD-gC pseudotype supports the use
366 of the pseudotyping platform developed here for future gain-of-function studies. In these future
367 studies, changes in tropism, entry routes, or both, may be uncovered.
368
369 ***VSVΔG-BHLD pseudotype has a narrower cellular tropism than HSV-1.*** HSV-1 can infect a
370 wide range of receptor-bearing cell types from different species [reviewed in (25)]. However, the
371 VSVΔG-BHLD pseudotype has a narrower tropism, efficiently entering only 2 out of 7 tested
372 cell lines. Puzzlingly, while VSVΔG-BHLD entered two engineered rodent cell lines, it exhibited
373 little to no entry into the four human and primate cell lines typically used in HSV-1 studies, even
374 at an MOI of 10. The lack of VSVΔG-BHLD entry did not correlate with the HSV-1 entry route
375 into these cells, namely, endocytosis for HeLa and HaCaT (5, 46) vs. plasma membrane for Vero
376 and SH-SY5Y (5, 44). Additionally, there was no clear correlation with the receptor type (nectin-
377 1 vs. HVEM) or with the cell type. While any of these factors – species, cell type, receptor, or
378 route of entry – could potentially account for the decreased entry efficiency observed for
379 VSVΔG-BHLD pseudotype, none stood out as major infectivity determinants.

380 We do not yet fully understand the reasons for the observed differences in tropism
381 between the VSVΔG-BHLD pseudotype and HSV-1. At a first glance, the differences in virion
382 structure – bullet-shaped vs. spherical – could be responsible for the phenotypic differences.
383 However, the apparent differences in the entry of VSVΔG-BHLD, VSVΔG-G, and VSVΔG-
384 PIV5 pseudotypes, all of which share the same VSV structure, suggest that virion structure is
385 unlikely to be a major factor responsible for the observed differences in entry of VSVΔG-BHLD
386 and HSV-1. The gB:gH:gL:gD ratios were also similar between VSVΔG-BHLD and HSV-1. The
387 two viruses could, however, differ in lipid composition because VSV and HSV-1 acquire their
388 envelopes from different sources. VSV buds at the plasma membrane (PM) (27) whereas HSV-1
389 buds at the trans-Golgi network (TGN) (42) or endosome-derived vesicles (43). However,
390 according to recent lipidomics studies, the PM, the TGN, and the endosomes have similar lipid
391 compositions (84). While we acknowledge that even small differences in lipid composition of the
392 envelope could potentially contribute to differences in entry routes, this line of inquiry is beyond
393 the scope of the present study. Moreover, no benchmarks are in place because HSV-1 lipid
394 composition is unknown and cannot be altered on demand.
395 Importantly, VSV pseudotypes have been successfully used to study the entry of
396 enveloped viruses regardless of the envelope origin. In addition to viruses that, like VSV, acquire
397 their envelopes from the plasma membrane (Ebola virus, Lassa virus, Lujo virus) (31-34),
398 viruses that derive their envelopes from the ER (Hepatitis C virus, Japanese encephalitis virus)
399 (37, 38) or the Golgi (Hantavirus, Rift Valley fever virus) (35, 36) have also been studied. These
400 observations suggest that VSV pseudotypes can provide important insights into viral entry
401 mechanisms regardless of envelope origins.

402 This leaves differences in glycoprotein content as a potential reason for the differences in
403 tropism. HSV-1 has up to 12 envelope proteins outside of the core set of four, which are absent
404 from VSVΔG-BHLD. We hypothesize that efficient entry by HSV-1 into susceptible cells
405 requires one or more of these other proteins. Indeed, some of them have already been shown to
406 increase HSV-1 entry efficiency. For example, deletion of the N terminus of glycoprotein K (gK)
407 promoted inefficient endocytic entry into Vero cells (85, 86), which normally support entry by
408 fusion at the plasma membrane (44). The N terminus of gK may thus regulate the fusion of the
409 viral envelope with the plasma membrane (85). Another HSV-1 glycoprotein, gC, aids viral
410 attachment by binding heparan sulfate moieties of cell surface proteoglycans (87) and promotes
411 efficient entry into cells that HSV-1 enters by an endocytic route (88). Thus, envelope proteins
412 outside of the core set of four could, indeed, modulate HSV-1 tropism by tuning entry efficiency.
413 In other words, the more efficiently HSV-1 enters a given cell type, the more likely that cell type
414 is to be successfully infected.
415 This hypothesis could be tested by adding the "non-essential" envelope proteins one-by-
416 one into the VSVΔG-BHLD pseudotype to test for their ability to restore entry into specific cell
417 lines. For example, the incorporation of gK into the VSVΔG-BHLD pseudotype (VSVΔG-
418 BHLD-gK) would be expected to increase the entry efficiency into cells that HSV-1 enters by
419 fusion at the plasma membrane (Vero and SH-SY5Y), whereas gC (VSVΔG-BHLD-gC) could
420 increase the entry efficiency into cells that HSV-1 enters by endocytosis (C10, CHO-nectin-1,
421 CHO-HVEM, HeLa and HaCaT). Indeed, we found that incorporating gC into the VSVΔG-
422 BHLD pseudotype increased entry efficiency into CHO-HVEM and HaCaT cells. These results
423 are consistent with the reduced entry efficiency of an HSV-1 mutant lacking gC into these cell

424 types (88). The mechanism underlying the gC-dependent gain-of-function phenotype of
425 VSVΔG-BHLD-gC will be explored in future work.
426
427 ***VSVΔG-BHLD pseudotype is internalized differently from HSV-1.*** If HSV-1 gB, gH, gL, and
428 gD were sufficient to specify the native routes of HSV-1 entry, then we would have expected the
429 VSVΔG-BHLD pseudotype to utilize the same entry routes into C10 and CHO-HVEM as HSV-
430 1. However, while entry of both viruses occurred by endocytosis and required dynamin and
431 cellular cholesterol but not caveolin-1 or actin polymerization, further investigation uncovered
432 several notable differences in entry requirements (Fig. 9).
433 The first difference was that HSV-1 entry into C10 or CHO-HVEM cells was inhibited
434 by the clathrin inhibitor Pitstop-2, suggesting that it occurred by CME, whereas VSVΔG-BHLD
435 entry was not. HSV-1 entry inhibition by Pitstop-2 was unexpected because HSV-1 does not
436 appear to utilize clathrin for entry into several cell lines, including HaCaT (89), CHO-nectin-1
437 (90), Vero, HeLaS3, and HeLaCNX cells (91). However, the role of clathrin in entry into C10 or
438 CHO-HVEM cells had not been assessed prior to this study. Moreover, recent work has
439 suggested that HSV-1 entry into a human oligodendrocytic cell line (HOG) depends on clathrin
440 (92). Therefore, HSV-1 may utilize CME in a cell-specific manner.
441 Unlike HSV-1 entry, VSVΔG-BHLD entry into C10 or CHO-HVEM cells was not
442 inhibited by Pitstop-2, which implicated CIE, rather than CME, as the entry route.
443 Macropinocytosis is a common CIE used by several viruses, but VSVΔG-BHLD entry into both
444 C10 and CHO-HVEM cells was insensitive to the inhibitor of actin polymerization, cytochalasin
445 D, as was HSV-1. Given the essential role of actin polymerization in macropinocytosis (68, 71),
446 these data suggest that macropinocytosis is not the primary entry mechanism for VSVΔG-BHLD

447 pseudotype or HSV-1. Accordingly, VSVΔG-BHLD particles did not colocalize with a fluid
448 phase uptake marker 70 kDa rhodamine-B-labeled dextran to an appreciable extent. The lack of
449 actin involvement in HSV-1 entry was not entirely surprising because its requirement, as deemed
450 by cytochalasin D treatment, varies from cell line to cell line. For example, cytochalasin D
451 treatment blocked entry into CHO-nectin-1 cells (90) but not into primary keratinocytes or
452 HaCaT cells (89).

453 Unexpectedly, VSVΔG-BHLD entry into both C10 and CHO-HVEM cells was sensitive
454 to two other inhibitors of macropinocytosis, EIPA and NSC23766. If the VSVΔG-BHLD
455 pseudotype does not enter cells by macropinocytosis, why is its entry sensitive to EIPA and
456 NSC23766? One possibility is that the respective targets of these inhibitors, Na^+/H^+ exchangers
457 and Rac1, could contribute to VSVΔG-BHLD entry independently of their roles in
458 macropinocytosis. For example, EIPA inhibits the function of other cellular GTPases like Rac1
459 and Cdc42 (69) whereas NSC23766 could affect other downstream targets of Rac1 [reviewed in
460 (93)]. Alternatively, EIPA and NSC23766 could inhibit VSVΔG-BHLD entry due to their
461 documented pleotropic effects on the cell. EIPA treatment can lead to a gross reorganization of
462 the endosomal network and changes in Na^+ and H^+ gradients in the cell (94, 95). Similarly, Rac1,
463 the target of NSC23766, is involved in several cellular processes in addition to regulating the
464 actin cytoskeleton (96).

465

466 ***VSVΔG-BHLD pseudotype and HSV-1 differ in late-stage entry requirements.*** Many viruses
467 that enter by endocytosis, for example, influenza A and VSV, rely on Rab-GTPase-dependent
468 endosomal maturation and acidification (74). VSVΔG-BHLD entry into C10 cells required Rab5,
469 an early endosome marker, and endosomal acidification. VSVΔG-BHLD entry into CHO-HVEM

470 cells and HSV-1 entry into both C10 and CHO-HVEM cells did not require either Rab5, or
471 Rab7, or endosomal acidification. Nevertheless, efficient entry of HSV-1 into both C10 and
472 CHO-HVEM cells required Arf6, a small GTPase involved in endosomal trafficking, including
473 CME and CIE (79). How Arf6 promotes HSV-1 entry is yet unclear considering its numerous
474 downstream effectors, including lipid modifying enzymes, proteins involved in endosome
475 trafficking, GTPase activating proteins (GAPs) and guanine exchange factors (GEFs) for other
476 GTPases [reviewed in (79)]. In contrast, Arf6 was dispensable for VSVΔG-BHLD entry.

477 One notable difference between VSVΔG-BHLD and HSV-1 entry into C10 cells was that
478 VSVΔG-BHLD entry required endosomal acidification. Previous work suggested that HSV-1
479 entry into C10 cells did not require endosomal acidification (45). Indeed, we confirmed that
480 HSV-1 entry into C10 cells was insensitive to bafilomycin A1 (BFLA), a well-known inhibitor
481 of endosomal acidification. The requirement for endosomal acidification for VSVΔG-BHLD
482 entry into C10 cells was unexpected. The membrane fusion itself may not require low pH, in
483 agreement with the observations that cell-cell fusion in the presence of gB, gH, gL, and gD
484 occurs at neutral pH (13). However, concomitant with the endosomal acidification, there are
485 significant changes in endosomal ion concentrations and lipid content (97), which could affect
486 membrane fusion or the fusion pore expansion. Therefore, we hypothesize that during VSVΔG-
487 BHLD entry, endosomal acidification promotes the establishment of endosomal conditions
488 conducive to fusion and that in HSV-1, envelope proteins outside the essential four may
489 functionally replace endosomal acidification.

490 Surprisingly, HSV-1 entry into both C10 and CHO-HVEM cells was inhibited by two
491 other inhibitors of endosomal acidification, NH_4Cl and monensin. Previous work showed that
492 HSV-1 entry into CHO-HVEM cells was sensitive to inhibitors of endosomal acidification

493 ammonium chloride (NH_4Cl) and monensin (46, 98), indicating a requirement for endosomal
494 acidification. While NH_4Cl and monensin alkalinize the lumen of endosomes, the mechanisms
495 by which they do so differ dramatically from BFLA. NH_4Cl, when dissolved, exists in
496 equilibrium as NH_3 and NH_4^+. Upon entering acidic environment, e.g., an endosome, NH_3
497 becomes protonated to NH_4^+, which leads to an increase in endosomal pH (97). Monensin is a
498 carboxylic ionophore that utilizes an electroneutral exchange of monovalent cations for protons,
499 effectively raising the endosomal pH (97). In parallel to these alkalinizing effects, NH_4Cl and
500 monensin can affect other cellular processes, e.g., vacuolization or organelle swelling. In
501 contrast, BFLA functions by specifically blocking the function of the V_0 domain of V-ATPases
502 thereby blocking the movement of protons across the endosomal membrane (99). At the nM
503 concentrations used, BFLA is very specific and potent in its action. Therefore, given that HSV-1
504 entry into either C10 or CHO-HVEM cells was not blocked by BFLA, we hypothesize that it
505 does not require endosomal acidification. Sensitivity of HSV-1 entry to NH_4Cl and monensin
506 could, instead, be due to their ability to interfere with other cellular processes. Both compounds
507 alter ion content of the endosomes and cause vacuolization (97). While the impact of endosome
508 vacuolization on HSV-1 entry has not been investigated, a change in endosomal ion
509 concentration could, potentially, reduce the ability of HSV-1 to fuse with the endosomal
510 membrane. Indeed, binding of HSV-1 to the cell surface releases intracellular Ca^{2+} stores (100)
511 and increases intracellular levels of Cl^- ions (101), both of which appear important for
512 subsequent entry.

513 Collectively, we hypothesize that HSV-1, which does not require Rab5/7 or endosomal
514 acidification, fuses with the endosomal membrane prior to maturation of the newly formed
515 vesicle into an early endosome [pH ~6.2 (102)] (Fig. 9). This latter scenario is consistent with

516 the rapid nature of HSV-1 entry into both C10 and B78A10 cells (B78 murine melanoma cells
517 expressing HVEM) cells ($t_{1/2}$ = 8-10 minutes) (45). Alternatively, endosomal maturation status
518 does not influence HSV-1 fusion with the membrane of the endocytic vesicle. VSVΔG-BHLD
519 entry into CHO-HVEM cells, likewise, does not require Rab5/7 or endosomal acidification,
520 implying that VSVΔG-BHLD may fuse with the endosomal membrane prior to delivery of the
521 endocytic vesicle to an early endosome. By contrast, VSVΔG-BHLD entry into C10 cells
522 requires both Rab5 and endosomal acidification, which suggests that VSVΔG-BHLD fuses with
523 membranes of early endosomes. This would suggest that during HSV-1 entry into C10 cells,
524 other envelope proteins may enable fusion prior to endosomal acidification.
525 As this and other studies show, HSV-1 entry is a complex phenomenon that requires at
526 least four glycoproteins (gB, gH, gL, and gD) that operate in the presence of up to 12 additional
527 envelope proteins, understudied with regard to entry. By establishing a platform where the
528 functionality of the four essential HSV-1 entry glycoproteins could be evaluated in isolation, we
529 demonstrated that they are insufficient to define HSV-1 tropism or specify native entry routes.
530 We have expanded the use of this platform by demonstrating that incorporation of an additional
531 envelope protein, gC, can lead to increased entry. Collectively, our work implicates other HSV-1
532 envelope proteins as underappreciated, yet potentially important contributors to HSV-1 tropism,
533 entry route selection, and, ultimately, pathogenesis.
534
535 **Materials and Methods**
536 ***Cells.*** HEK293T (gift from John Coffin, Tufts University), Vero (ATCC® CCL-81™), HeLa
537 (ATCC® CCL-2™), and HaCaT cells (gift from Jonathan Garlick, Tufts University) were grown
538 in Dulbecco's modified Eagle medium (DMEM; Lonza) containing high glucose, and sodium

539 pyruvate, supplemented with L-glutamine (Caisson Labs), 10% heat inactivated fetal bovine
540 serum (HI-FBS; Life Technologies) and 1X penicillin/streptomycin (pen/strep) solution
541 (Corning). B78H1 cells (a gift from Gary Cohen, University of Pennsylvania) were grown in
542 DMEM containing high glucose, sodium pyruvate, and L-glutamine supplemented with 5% FBS
543 and pen/strep solution (1X). C10 cells (a gift from Gary Cohen, University of Pennsylvania), a
544 clonal B78H1-derivative stably expressing human nectin-1, were grown in DMEM containing
545 high glucose, sodium pyruvate, and L-glutamine supplemented with 5% FBS and pen/strep
546 solution (1X) and maintained under selection for nectin-1 expression with 250 μg/ml of G418
547 (Selleck Chemical) as done previously (39). CHO-K1 cells were grown in Ham's F12 medium
548 containing 10% FBS and pen/strep solution (1X). CHO-HVEM cells, a derivative of CHO-K1
549 cells that stably express human HVEM, were grown in Ham's F12 medium containing 10% FBS
550 and penicillin-streptomycin solution (1X), 250 ug/ml G418 and 150 ug/ml of puromycin (AG
551 Scientific). CHO-K1 and CHO-HVEM cells were a gift from Anthony Nicola (Washington State
552 University). CHO-nectin-1 cells, a derivative of CHO-K1 cells that stably express human nectin-
553 1 were grown in Ham's F12 medium containing 10% FBS and penicillin-streptomycin solution
554 (1X), 250 ug/ml G418 and 5 ug/ml of puromycin (AG Scientific). CHO-nectin-1 cells were a gift
555 from Richard Longnecker (Northwestern University). SH-SY5Y cells were maintained in
556 EMEM (Sigma-Aldrich) supplemented with 15% HI-FBS and 1X penicillin/streptomycin. SH-
557 SY5Y cells were a kind gift from Stephen Moss (Tufts University).
558
559 ***Plasmids***. Plasmids pPEP98, pPEP99, pPEP100, and pPEP101 carry the full-length HSV-1
560 (strain KOS) genes for gB, gD, gH, and gL, respectively in a pCAGGS vector background.
561 These were kindly gifted by P.G. Spear (Northwestern University). pCMV-VSV-G, which

562 contains the full-length gene for the VSV glycoprotein, G, was a gift from Judith White
563 (University of Virginia). Rab GTPase dominant negative constructs [mCherry-Rab5DN(S34N)
564 and dsRed-Rab7DN] were purchased from Addgene (76, 77). For consistency, the dsRed in
565 dsRed-Rab7DN was replaced with mCherry by amplifying mCherry with the following primers:
566 5'-AGCGCTACCGGTCGCCACCATGGTGAGCAAGGGCGAG-3' (forward) and 5'-
567 AATTCGAAGCTTGAGCTCGAGATCTGAGCTTGTACAGCTCGTCCATGCC-3' (reverse).
568 mCherry was then cloned in frame with Rab7DN using AgeI and HindIII cut sites that were
569 engineered into the forward and reverse primers, respectively. As our HSV-1 reporter strain uses
570 tdTomato, eGFP-RabDN constructs were engineered. The same primers were used to amplify
571 eGFP from pEGFP-N2. The same cloning procedure was used to replace mCherry and dsRed
572 with eGFP in the Rab5DN and Rab7DN constructs, respectively. Isolated clones were sequenced
573 to verify mCherry and eGFP were in frame with the DN Rab genes. HSV-1 gC was amplified
574 from HSV-1 (F strain) BAC DNA (GS6000) with the following primers: 5'-
575 CGAGCTCGGCCACCATGGCCCCGGGGCGGG-3' (forward) and 5'-
576 GGGGTACCCCTCACGTAGAATCGAGACCGAGGAGAGGGTTAGGGATAGGCTTACCC
577 CGCCGATGACGCTGCCG-3' (reverse). The amplicon was digested with SacI and KpnI and
578 cloned into the expression vector, pCAGGS. The C-terminus of gC was tagged with a V5
579 epitope tag for western blot purposes.
580
581 ***Antibodies.*** Nectin-1 antibody [clone CK41 (103)] conjugated to phycoerythrin (PE) was
582 purchased from BD Biosciences. PE-isotype antibody was also purchased from BD Biosciences.
583 HVEM antibody (R140) was a gift from Gary Cohen (University of Pennsylvania). Caveolin-1
584 antibody (clone 4H312) was purchased from Santa Cruz Biotechnology. β-actin antibody

585 conjugated to horse radish peroxidase(sc-47778 HRP) was purchased from Santa Cruz
586 Biotechnology. Anti-V5 antibody (V8137) was purchased from Sigma-Aldrich.
587
588 ***Chemical inhibitors***. Monensin, methyl-β-cyclodextrin, cytochalasin D, Pitstop-2, and EIPA
589 were purchased from Sigma. Dynasore and MiTMAB were purchased from Calbiochem.
590 Bafilomycin A1 was purchased from ApexBio. Ammonium chloride was purchased from Fisher
591 Scientific. Dyngo-4a was purchased from Abcam. NSC23766 was purchased from Santa Cruz
592 Biotechnology.
593
594 ***Viruses.*** Pseudotyped viral particles (VSVΔG-BHLD) were generated as described previously
595 (39). Briefly, HEK293T cells (5.5 x 10^6 cells/10 cm dish) were transfected with 2.5 μg each
596 pPEP98, pPEP99, pPEP100, and pPEP101 using polyethyleneimine (PEI at 1 mg/ml) at a 3:1
597 weight ratio of PEI to DNA. VSVΔG-BHLD-pCAGGS and VSVΔG-BHLD-gC were generated
598 by transfecting HEK293T cells with 10 μg pPEP98 and 2.5 μg each of pPEP99, pPEP100,
599 pPEP101, and pCAGGS or pCAGGS-gC-V5 using GenJet Ver. II (SignaGen Laboratories). In
600 all cases, 24 hours post transfection, cells were infected at an MOI = 3 with VSVΔG-G (VSVΔG
601 pseudotyped with VSV G protein) and incubated at 30° C. Forty-eight hours post infection,
602 supernatants were collected, cleared of cell debris (two spins at 1500 x g for 10 minutes each),
603 and stored at -80° C. VSVΔG-BHLD, VSVΔG-BHLD-pCAGGS, and VSVΔG-BHLD-gC titers
604 were determined on C10 cells.
605 HSV-1 (GS3217, F strain) was kindly provided by Gregory Smith (Northwestern
606 University). GS3217 contains a tdTomato reporter gene with a nuclear localization signal under
607 control of a CMV immediate early (IE) promoter (104). HSV-1 was propagated on Vero cells,

608 and titers were determined by plaque assay on Vero cells as previously described (105).
609 VSVΔG-G helper virus was generated by Michael Whitt (University of Tennessee) and kindly
610 provided by Judith White (University of Virginia). New stocks were generated similarly to the
611 VSVΔG-BHLD pseudotypes, replacing the HSV-1 glycoproteins with pCMV-VSV-G (10 μg per
612 10 cm dish). VSVΔG-G titers were determined on C10 cells. VSVΔG-PIV5 was generated and
613 kindly provided by S.P.J. Whelan (Washington University). As VSVΔG-PIV5 contains the PIV5
614 HN and F proteins in the VSV genome, no complementation *in trans* was necessary. VSVΔG-
615 PIV5 was grown on HEK293T cells and titers were determined on C10 cells. Entry of the VSV
616 pseudotypes (VSVΔG-BHLD, VSVΔG-G, VSVΔG-PIV5, VSVΔG-BHLD-pCAGGS, and
617 VSVΔG-BHLD-gC) was assessed by the expression of the GFP reporter driven by the promoter
618 within the 3' leader sequence of the VSV genome.
619
620 ***Entry experiments.*** $3x10^5$ B78H1, C10, CHO-K1, CHO-nectin-1, CHO-HVEM, HeLa, HaCaT,
621 Vero, or SH-SY5Y cells were seeded in 35 mm dishes. Cells were infected with viruses at a
622 MOI=1. Viruses were incubated with cells at 37° C for one hour. After one hour, viruses that had
623 not entered were inactivated with a low pH wash (40 mM Na citrate, 10 mM KCl, 135 mM
624 NaCl, pH 3.0). Complete growth media was added back to cells and infections were allowed to
625 progress for six hours prior to analysis by flow cytometry. Entry experiments in the presence of
626 inhibitors were performed similarly except that prior to infection, C10 and CHO-HVEM cells
627 were pretreated with the indicated inhibitors for one hour prior to infection. All inhibitors, with
628 the exception of sucrose and methyl-β-cyclodextrin, were present during the infection and the six
629 hours post infection prior to analysis by flow cytometry by measuring tdTomato expression

630 (HSV-1 GS3217) or EGFP expression (VSV pseudotypes) to allow sufficient time for viral entry
631 and expression of the fluorescent reporters.
632 Viral entry experiments in the presence of fluorescently labeled Rab GTPase dominant
633 negative constructs were performed and analyzed as follows: cells infected with HSV-1
634 (tdTomato) were transfected with pEGFP-N2 as an empty vector control or eGFP-tagged RabDN
635 constructs whereas cells infected with VSV pseudotypes (eGFP) were transfected with
636 pmCherry-C1 empty vector control or mCherry-tagged RabDN constructs. The data are
637 represented as the percentage of infected and transfected cells out of the total number of
638 transfected cells with either the empty vector control or the RabDN constructs.
639 Prior to flow cytometry analysis, cells were trypsinized, resuspended in media and
640 pelleted at 450 x g for five minutes. Cells were washed with 1X PBS containing 1 mM EDTA (to
641 prevent clumping). Cells were pelleted again at 450 x g for five minutes. Cells were then
642 resuspended in 1X PBS with 1 mM EDTA and transferred to FACS tubes. Flow cytometry was
643 performed on a BD LSR II or FACSCalibur instrument. tdTomato expression (HSV-1 GS3217)
644 or EGFP expression (VSV pseudotypes) were measured as a proxy for viral entry. Data analysis
645 was done using FlowJo software (v. 8.8.7).
646
647 ***Analyses of receptor expression by flow cytometry.*** Nectin-1 was detected on the surface of cells
648 by staining them with anti-nectin-1 antibody CK41 conjugated to PE (BD Biosciences). HVEM
649 was detected on the surface of cells using the anti-HVEM polyclonal antibody, R140, a gift from
650 Gary Cohen (University of Pennsylvania), and a FITC-conjugated anti-rabbit secondary antibody
651 (ThermoFisher). Briefly, $1x10^6$ cells were plated into 10 cm dishes. The next day, cells were
652 lifted from the dishes with 1X-PBS containing 5 mM EDTA. Cells were then pelleted,

653 resuspended in 300 μl FACS buffer (1X-PBS, 2% FBS, 1 mM EDTA), and divided evenly
654 between microfuge tubes for mock, PE-isotype, or PE-anti-nectin-1 treatment. Cells were
655 incubated with 1 μg of antibody for 30 minutes on ice with agitation every 10 minutes. Similarly,
656 cells were divided for mock, isotype (anti-gB R68 polyclonal antibody), or R140 anti-HVEM
657 treatment. Cells were incubated with 5 μg of antibody. Mock, isotype, and R140-labeled cells
658 were then incubated with a FITC-conjugated anti-rabbit secondary antibody (ThermoFisher).
659 After 30 minutes, cells were pelleted and washed three times with FACS buffer, re-suspended,
660 then immediately analyzed by flow cytometry (FACSCalibur).
661
662 ***Virus purification and densitometry analysis.*** HSV-1 and VSVΔG-BHLD virions were purified
663 and subjected to immunoblot for gB, gH, gL, and gD. Briefly, five T-175 flasks of Vero cells
664 were infected with HSV-1 (MOI 0.01). HSV-1 was crudely purified as previously described
665 (105). HSV-1 particles were then purified over a continuous 15-50% sucrose gradient (106). The
666 purified band of HSV-1 was collected by puncture and aspiration. VSVΔG-BHLD virions were
667 generated as previously mentioned (see *Viruses* section of Materials and Methods). VSVΔG-
668 BHLD particles were then pelleted at 20,000 RPM. VSVΔG-BHLD virions were then
669 resuspended and purified over a continuous 15-35% Optiprep gradient [protocol adapted from
670 (107, 108)] and collected by puncture and aspiration. HSV-1 and VSVΔG-BHLD virions were
671 pelleted at 20,0000 RPM. Western blots for gB, gH, gL, and gD were done using the rabbit
672 polyclonal R68 antibody (gB), the rabbit polyclonal R137 antibody (gH), the mouse monoclonal
673 antibody L1 (gL), and the rabbit polyclonal antibody R7 (gD). Secondary antibodies from LI-
674 COR were used in order to perform densitometry analysis using the Image Studio Lite software
675 (IRDye® 680RD goat anti-rabbit and IRDye® 800CW goat anti-mouse). Raw densitometry

676 values for gH, gL, and gD blots were normalized to their respective raw densitometry values for
677 gB and reported as fold-differences to gB.
678
679 ***Confocal microscopy.*** $1x10^5$ cells (C10 and CHO-HVEM) were seeded onto 12 mm glass
680 coverslips (Chemglass) in 24 well plates. Prior to labeling cells with specific markers of different
681 endocytosis pathways, cells were pretreated with inhibitors for one hour at 37 °C. Post pre-
682 treatment, cells were chilled to 4 °C for 10-15 minutes and were subsequently incubated with
683 specific endocytic markers: Transferrin-Alexa Fluor 488 (50 μg/ml, Thermo Fisher Scientific),
684 70-kD dextran-rhodamine B (1 mg/ml, Thermo Fisher Scientific), or Lysotracker (1 μM, Thermo
685 Fisher Scientific). Cells were incubated with endocytic markers for 10 minutes at 4° C. After the
686 10-minute incubation, C10 cells were shifted to 37° C for 10 minutes and CHO-HVEM cells
687 were shifted to 37° C for 30 minutes (Transferrin-Alexa Fluor 488 and Lysotracker) or 40
688 minutes (70 kDa dextran) (109). After incubation at 37° C, cells were washed 3 times with 1X-
689 PBS and fixed in 4% paraformaldehyde for 15 minutes at room temperature. Cells were washed
690 three times with 1X-PBS and incubated with 2.5 μg/ml of DAPI (ThermoFisher Scientific)
691 diluted in 1X-PBS for 15 minutes at room temperature. Cells were washed again three times with
692 1X-PBS and mounted onto Prolong Gold Antifade (Life Technologies) on glass slides (Thermo
693 Fisher Scientific). Coverslips were sealed with clear nail polish and analyzed by confocal
694 microscopy using a Leica SPE microscope. Images were analyzed in Fiji (110). For 70-kDa
695 dextran and VSVΔG-BHLD co-localization experiments, C10 and CHO-HVEM cells were
696 incubated with 1 mg/ml 70 kDa dextran and VSVΔG-BHLD (MOI = 1) for 1 hour at 4° C to
697 allow for virion attachment. Cells were then shifted to 37° C for 20 minutes. After 20 minutes,

698 cells were prepared for confocal microscopy by fixing with 4% paraformaldehyde, permeabilized
699 and blocked with 1X PBS containing 5% normal goat serum and 0.3% Triton X-100. Cells were
700 then incubated with anti-gB antibody (R68) overnight at 4° C. The next day, cells were incubated
701 with a secondary antibody labeled with FITC for 1 hour at room temperature. Slides were then
702 prepared as described above.
703
704 ***siRNA-mediated knockdown.*** Mouse caveolin-1 siRNA, and a control siRNA were purchased
705 from Santa Cruz Biotechnologies. 50 pmol of siRNA (0.625 μg) (cav-1 or scramble [scr]) were
706 diluted into 100 μl of Optimem. In another tube, 3.125 μl of PEI (1 mg/ml) was diluted into 100
707 μl of Optimem. The diluted PEI was mixed with the diluted siRNA to a final ratio of 5:1 (w:w)
708 of PEI to siRNA and incubated at room temperature for 30 minutes. The complex was added
709 dropwise to CHO-HVEM cells plated in 35 mm dishes (3 x 10^5 cells/dish). Cells were incubated
710 at 37° C for 48 hours before infection and subsequent flow cytometry analysis.
711
712 **Acknowledgments**
713 We thank Stephen Kwok and Allen Parmelee at the Tufts Laser Cytometry Core facility for their
714 help with FACS experiments; Gary Cohen (University of Pennsylvania) for the gifts of
715 antibodies and cell lines; Sean Whelan (Washington University) for the gift of VSVΔG-PIV5
716 pseudotype; Anthony Nicola (Washington State University) for the gift of CHO-K1 and CHO-
717 HVEM cells; Richard Longnecker (Northwestern University) for the gift of CHO-nectin-1 cells;
718 John Coffin (Tufts University) for the gift of HEK293T cells; Stephen Moss (Tufts University)
719 for the gift of SH-SY5Y cells; Jonathan Garlick (Tufts University) for the gift of HaCaT cells;
720 Michael Forgac (Tufts University) for the gift of Lysotracker reagent; Gregory Smith

721 (Northwestern University) for the gift of HSV-1 GS3217 strain, and Michael Whitt (University
722 of Tennessee) and Judith White (University of Virginia) for the gift of the VSVΔG-GFP
723 pseudotyping platform. FACS experiments were performed at the Tufts Laser Cytometry Core
724 facility.

725

726 **Competing Interests**

727 The authors declare no competing interests.

728

729 **Data sharing plan**

730 All data is included in the manuscript and supporting information.

731

732 **Funding information**

733 This work was funded by the NIH grant R21AI140711 (E.E.H.), a Faculty Scholar grant
734 55108533 from Howard Hughes Medical Institute (E.E.H.), and the NIH training grant
735 T32AI007329 (A.T.H.).

736

737 **References**

738 1. Steiner I, Benninger F. 2013. Update on herpes virus infections of the nervous system.
739 Curr Neurol Neurosci Rep 13:414.
740 2. Bradley H, Markowitz LE, Gibson T, McQuillan GM. 2014. Seroprevalence of herpes
741 simplex virus types 1 and 2--United States, 1999-2010. J Infect Dis 209:325-33.
742 3. Agelidis AM, Shukla D. 2015. Cell entry mechanisms of HSV: what we have learned in
743 recent years. Future Virol 10:1145-1154.
744 4. Miranda-Saksena M, Denes CE, Diefenbach RJ, Cunningham AL. 2018. Infection and
745 Transport of Herpes Simplex Virus Type 1 in Neurons: Role of the Cytoskeleton. Viruses
746 10.
747 5. Nicola AV, Hou J, Major EO, Straus SE. 2005. Herpes simplex virus type 1 enters human
748 epidermal keratinocytes, but not neurons, via a pH-dependent endocytic pathway. J Virol
749 79:7609-16.

750 6. Cai WH, Gu B, Person S. 1988. Role of glycoprotein B of herpes simplex virus type 1 in
751 viral entry and cell fusion. J Virol 62:2596-604.
752 7. Roop C, Hutchinson L, Johnson DC. 1993. A mutant herpes simplex virus type 1 unable
753 to express glycoprotein L cannot enter cells, and its particles lack glycoprotein H. J Virol
754 67:2285-97.
755 8. Ligas MW, Johnson DC. 1988. A herpes simplex virus mutant in which glycoprotein D
756 sequences are replaced by beta-galactosidase sequences binds to but is unable to
757 penetrate into cells. J Virol 62:1486-94.
758 9. Heldwein EE, Krummenacher C. 2008. Entry of herpesviruses into mammalian cells.
759 Cell Mol Life Sci 65:1653-68.
760 10. Connolly SA, Jackson JO, Jardetzky TS, Longnecker R. 2011. Fusing structure and
761 function: a structural view of the herpesvirus entry machinery. Nat Rev Microbiol 9:369-
762 81.
763 11. Muggeridge MI. 2000. Characterization of cell-cell fusion mediated by herpes simplex
764 virus 2 glycoproteins gB, gD, gH and gL in transfected cells. J Gen Virol 81:2017-27.
765 12. Turner A, Bruun B, Minson T, Browne H. 1998. Glycoproteins gB, gD, and gHgL of
766 herpes simplex virus type 1 are necessary and sufficient to mediate membrane fusion in a
767 Cos cell transfection system. J Virol 72:873-5.
768 13. Atanasiu D, Saw WT, Cohen GH, Eisenberg RJ. 2010. Cascade of events governing cell-
769 cell fusion induced by herpes simplex virus glycoproteins gD, gH/gL, and gB. J Virol
770 84:12292-9.
771 14. Eisenberg RJ, Atanasiu D, Cairns TM, Gallagher JR, Krummenacher C, Cohen GH.
772 2012. Herpes virus fusion and entry: a story with many characters. Viruses 4:800-32.
773 15. Spear PG, Eisenberg RJ, Cohen GH. 2000. Three classes of cell surface receptors for
774 alphaherpesvirus entry. Virology 275:1-8.
775 16. Krummenacher C, Supekar VM, Whitbeck JC, Lazear E, Connolly SA, Eisenberg RJ,
776 Cohen GH, Wiley DC, Carfi A. 2005. Structure of unliganded HSV gD reveals a
777 mechanism for receptor-mediated activation of virus entry. EMBO J 24:4144-53.
778 17. Lazear E, Carfi A, Whitbeck JC, Cairns TM, Krummenacher C, Cohen GH, Eisenberg
779 RJ. 2008. Engineered disulfide bonds in herpes simplex virus type 1 gD separate receptor
780 binding from fusion initiation and viral entry. J Virol 82:700-9.
781 18. Cairns TM, Ditto NT, Atanasiu D, Lou H, Brooks BD, Saw WT, Eisenberg RJ, Cohen
782 GH. 2019. Surface Plasmon Resonance Reveals Direct Binding of Herpes Simplex Virus
783 Glycoproteins gH/gL to gD and Locates a gH/gL Binding Site on gD. J Virol 93.
784 19. Atanasiu D, Cairns TM, Whitbeck JC, Saw WT, Rao S, Eisenberg RJ, Cohen GH. 2013.
785 Regulation of Herpes Simplex Virus gB-Induced Cell-Cell Fusion by Mutant Forms of
786 gH/gL in the Absence of gD and Cellular Receptors. Mbio 4.
787 20. Gianni T, Amasio M, Campadelli-Fiume G. 2009. Herpes simplex virus gD forms
788 distinct complexes with fusion executors gB and gH/gL in part through the C-terminal
789 profusion domain. J Biol Chem 284:17370-82.
790 21. Atanasiu D, Whitbeck JC, de Leon MP, Lou H, Hannah BP, Cohen GH, Eisenberg RJ.
791 2010. Bimolecular complementation defines functional regions of Herpes simplex virus
792 gB that are involved with gH/gL as a necessary step leading to cell fusion. J Virol
793 84:3825-34.

794 22. Chowdary TK, Cairns TM, Atanasiu D, Cohen GH, Eisenberg RJ, Heldwein EE. 2010.
795 Crystal structure of the conserved herpesvirus fusion regulator complex gH-gL. Nat
796 Struct Mol Biol 17:882-8.
797 23. Cooper RS, Heldwein EE. 2015. Herpesvirus gB: A Finely Tuned Fusion Machine.
798 Viruses 7:6552-69.
799 24. Loret S, Guay G, Lippe R. 2008. Comprehensive characterization of extracellular herpes
800 simplex virus type 1 virions. J Virol 82:8605-18.
801 25. Karasneh GA, Shukla D. 2011. Herpes simplex virus infects most cell types in vitro:
802 clues to its success. Virol J 8:481.
803 26. Hilterbrand AT, Heldwein EE. 2019. Go go gadget glycoprotein!: HSV-1 draws on its
804 sizeable glycoprotein tool kit to customize its diverse entry routes. PLoS Pathog
805 15:e1007660.
806 27. Whitt MA. 2010. Generation of VSV pseudotypes using recombinant DeltaG-VSV for
807 studies on virus entry, identification of entry inhibitors, and immune responses to
808 vaccines. J Virol Methods 169:365-74.
809 28. Fukushi S, Mizutani T, Saijo M, Matsuyama S, Miyajima N, Taguchi F, Itamura S,
810 Kurane I, Morikawa S. 2005. Vesicular stomatitis virus pseudotyped with severe acute
811 respiratory syndrome coronavirus spike protein. J Gen Virol 86:2269-2274.
812 29. Fukushi S, Watanabe R, Taguchi F. 2008. Pseudotyped vesicular stomatitis virus for
813 analysis of virus entry mediated by SARS coronavirus spike proteins. Methods Mol Biol
814 454:331-8.
815 30. Nie J, Li Q, Wu J, Zhao C, Hao H, Liu H, Zhang L, Nie L, Qin H, Wang M, Lu Q, Li X,
816 Sun Q, Liu J, Fan C, Huang W, Xu M, Wang Y. 2020. Establishment and validation of a
817 pseudovirus neutralization assay for SARS-CoV-2. Emerg Microbes Infect 9:680-686.
818 31. Carette JE, Raaben M, Wong AC, Herbert AS, Obernosterer G, Mulherkar N, Kuehne AI,
819 Kranzusch PJ, Griffin AM, Ruthel G, Dal Cin P, Dye JM, Whelan SP, Chandran K,
820 Brummelkamp TR. 2011. Ebola virus entry requires the cholesterol transporter Niemann-
821 Pick C1. Nature 477:340-3.
822 32. Jae LT, Raaben M, Riemersma M, van Beusekom E, Blomen VA, Velds A, Kerkhoven
823 RM, Carette JE, Topaloglu H, Meinecke P, Wessels MW, Lefeber DJ, Whelan SP, van
824 Bokhoven H, Brummelkamp TR. 2013. Deciphering the glycosylome of
825 dystroglycanopathies using haploid screens for lassa virus entry. Science 340:479-83.
826 33. Jae LT, Raaben M, Herbert AS, Kuehne AI, Wirchnianski AS, Soh TK, Stubbs SH,
827 Janssen H, Damme M, Saftig P, Whelan SP, Dye JM, Brummelkamp TR. 2014. Virus
828 entry. Lassa virus entry requires a trigger-induced receptor switch. Science 344:1506-10.
829 34. Raaben M, Jae LT, Herbert AS, Kuehne AI, Stubbs SH, Chou YY, Blomen VA,
830 Kirchhausen T, Dye JM, Brummelkamp TR, Whelan SP. 2017. NRP2 and CD63 Are
831 Host Factors for Lujo Virus Cell Entry. Cell Host Microbe 22:688-696 e5.
832 35. Kleinfelter LM, Jangra RK, Jae LT, Herbert AS, Mittler E, Stiles KM, Wirchnianski AS,
833 Kielian M, Brummelkamp TR, Dye JM, Chandran K. 2015. Haploid Genetic Screen
834 Reveals a Profound and Direct Dependence on Cholesterol for Hantavirus Membrane
835 Fusion. mBio 6:e00801.
836 36. Riblett AM, Blomen VA, Jae LT, Altamura LA, Doms RW, Brummelkamp TR,
837 Wojcechowskyj JA. 2016. A Haploid Genetic Screen Identifies Heparan Sulfate
838 Proteoglycans Supporting Rift Valley Fever Virus Infection. J Virol 90:1414-23.

839 37. Tani H, Komoda Y, Matsuo E, Suzuki K, Hamamoto I, Yamashita T, Moriishi K,
840 Fujiyama K, Kanto T, Hayashi N, Owsianka A, Patel AH, Whitt MA, Matsuura Y. 2007.
841 Replication-competent recombinant vesicular stomatitis virus encoding hepatitis C virus
842 envelope proteins. J Virol 81:8601-12.
843 38. Tani H, Morikawa S, Matsuura Y. 2011. Development and Applications of VSV Vectors
844 Based on Cell Tropism. Front Microbiol 2:272.
845 39. Rogalin HB, Heldwein EE. 2016. Characterization of Vesicular Stomatitis Virus
846 Pseudotypes Bearing Essential Entry Glycoproteins gB, gD, gH, and gL of Herpes
847 Simplex Virus 1. J Virol 90:10321-10328.
848 40. Robinson LR, Whelan SP. 2016. Infectious Entry Pathway Mediated by the Human
849 Endogenous Retrovirus K Envelope Protein. J Virol 90:3640-9.
850 41. Krummenacher C, Baribaud F, Ponce de Leon M, Baribaud I, Whitbeck JC, Xu R, Cohen
851 GH, Eisenberg RJ. 2004. Comparative usage of herpesvirus entry mediator A and nectin-
852 1 by laboratory strains and clinical isolates of herpes simplex virus. Virology 322:286-99.
853 42. Henaff D, Radtke K, Lippe R. 2012. Herpesviruses exploit several host compartments for
854 envelopment. Traffic 13:1443-9.
855 43. Hollinshead M, Johns HL, Sayers CL, Gonzalez-Lopez C, Smith GL, Elliott G. 2012.
856 Endocytic tubules regulated by Rab GTPases 5 and 11 are used for envelopment of
857 herpes simplex virus. EMBO J 31:4204-20.
858 44. Koyama AH, Uchida T. 1987. The mode of entry of herpes simplex virus type 1 into
859 Vero cells. Microbiol Immunol 31:123-30.
860 45. Milne RS, Nicola AV, Whitbeck JC, Eisenberg RJ, Cohen GH. 2005. Glycoprotein D
861 receptor-dependent, low-pH-independent endocytic entry of herpes simplex virus type 1.
862 J Virol 79:6655-63.
863 46. Nicola AV, McEvoy AM, Straus SE. 2003. Roles for endocytosis and low pH in herpes
864 simplex virus entry into HeLa and Chinese hamster ovary cells. J Virol 77:5324-32.
865 47. Dutta D, Donaldson JG. 2012. Search for inhibitors of endocytosis: Intended specificity
866 and unintended consequences. Cell Logist 2:203-208.
867 48. Carpentier JL, Sawano F, Geiger D, Gorden P, Perrelet A, Orci L. 1989. Potassium
868 depletion and hypertonic medium reduce "non-coated" and clathrin-coated pit formation,
869 as well as endocytosis through these two gates. J Cell Physiol 138:519-26.
870 49. Bose S, Zokarkar A, Welch BD, Leser GP, Jardetzky TS, Lamb RA. 2012. Fusion
871 activation by a headless parainfluenza virus 5 hemagglutinin-neuraminidase stalk
872 suggests a modular mechanism for triggering. Proc Natl Acad Sci U S A 109:E2625-34.
873 50. Matlin KS, Reggio H, Helenius A, Simons K. 1982. Pathway of vesicular stomatitis virus
874 entry leading to infection. J Mol Biol 156:609-31.
875 51. Superti F, Seganti L, Ruggeri FM, Tinari A, Donelli G, Orsi N. 1987. Entry pathway of
876 vesicular stomatitis virus into different host cells. J Gen Virol 68 (Pt 2):387-99.
877 52. Johannsdottir HK, Mancini R, Kartenbeck J, Amato L, Helenius A. 2009. Host cell
878 factors and functions involved in vesicular stomatitis virus entry. J Virol 83:440-53.
879 53. Marsh M, Helenius A. 2006. Virus entry: open sesame. Cell 124:729-40.
880 54. Mercer J, Schelhaas M, Helenius A. 2010. Virus entry by endocytosis. Annu Rev
881 Biochem 79:803-33.
882 55. Kirchhausen T. 2000. Clathrin. Annu Rev Biochem 69:699-727.
883 56. Singh M, Jadhav HR, Bhatt T. 2017. Dynamin Functions and Ligands: Classical
884 Mechanisms Behind. Mol Pharmacol 91:123-134.

885 57. Quan A, McGeachie AB, Keating DJ, van Dam EM, Rusak J, Chau N, Malladi CS, Chen
886 C, McCluskey A, Cousin MA, Robinson PJ. 2007. Myristyl trimethyl ammonium
887 bromide and octadecyl trimethyl ammonium bromide are surface-active small molecule
888 dynamin inhibitors that block endocytosis mediated by dynamin I or dynamin II. Mol
889 Pharmacol 72:1425-39.
890 58. Cureton DK, Massol RH, Saffarian S, Kirchhausen TL, Whelan SP. 2009. Vesicular
891 stomatitis virus enters cells through vesicles incompletely coated with clathrin that
892 depend upon actin for internalization. PLoS Pathog 5:e1000394.
893 59. Mayor S, Parton RG, Donaldson JG. 2014. Clathrin-independent pathways of
894 endocytosis. Cold Spring Harb Perspect Biol 6.
895 60. Pelkmans L, Kartenbeck J, Helenius A. 2001. Caveolar endocytosis of simian virus 40
896 reveals a new two-step vesicular-transport pathway to the ER. Nat Cell Biol 3:473-83.
897 61. Xu Q, Cao M, Song H, Chen S, Qian X, Zhao P, Ren H, Tang H, Wang Y, Wei Y, Zhu
898 Y, Qi Z. 2016. Caveolin-1-mediated Japanese encephalitis virus entry requires a two-step
899 regulation of actin reorganization. Future Microbiol 11:1227-1248.
900 62. Williams TM, Lisanti MP. 2004. The caveolin proteins. Genome Biol 5:214.
901 63. de Almeida CJG. 2017. Caveolin-1 and Caveolin-2 Can Be Antagonistic Partners in
902 Inflammation and Beyond. Front Immunol 8:1530.
903 64. Bender FC, Whitbeck JC, Ponce de Leon M, Lou H, Eisenberg RJ, Cohen GH. 2003.
904 Specific association of glycoprotein B with lipid rafts during herpes simplex virus entry. J
905 Virol 77:9542-52.
906 65. Chinnapen DJ, Chinnapen H, Saslowsky D, Lencer WI. 2007. Rafting with cholera toxin:
907 endocytosis and trafficking from plasma membrane to ER. FEMS Microbiol Lett
908 266:129-37.
909 66. Danthi P, Chow M. 2004. Cholesterol removal by methyl-beta-cyclodextrin inhibits
910 poliovirus entry. J Virol 78:33-41.
911 67. Dou X, Li Y, Han J, Zarlenga DS, Zhu W, Ren X, Dong N, Li X, Li G. 2018. Cholesterol
912 of lipid rafts is a key determinant for entry and post-entry control of porcine rotavirus
913 infection. BMC Vet Res 14:45.
914 68. Mercer J, Helenius A. 2009. Virus entry by macropinocytosis. Nat Cell Biol 11:510-20.
915 69. Koivusalo M, Welch C, Hayashi H, Scott CC, Kim M, Alexander T, Touret N, Hahn
916 KM, Grinstein S. 2010. Amiloride inhibits macropinocytosis by lowering
917 submembranous pH and preventing Rac1 and Cdc42 signaling. J Cell Biol 188:547-63.
918 70. Gao Y, Dickerson JB, Guo F, Zheng J, Zheng Y. 2004. Rational design and
919 characterization of a Rac GTPase-specific small molecule inhibitor. Proc Natl Acad Sci
920 U S A 101:7618-23.
921 71. Hansen CG, Nichols BJ. 2009. Molecular mechanisms of clathrin-independent
922 endocytosis. J Cell Sci 122:1713-21.
923 72. Cureton DK, Massol RH, Whelan SP, Kirchhausen T. 2010. The length of vesicular
924 stomatitis virus particles dictates a need for actin assembly during clathrin-dependent
925 endocytosis. PLoS Pathog 6:e1001127.
926 73. Spearman P. 2018. Viral interactions with host cell Rab GTPases. Small GTPases 9:192-
927 201.
928 74. Sieczkarski SB, Whittaker GR. 2003. Differential requirements of Rab5 and Rab7 for
929 endocytosis of influenza and other enveloped viruses. Traffic 4:333-43.

930 75. Langemeyer L, Frohlich F, Ungermann C. 2018. Rab GTPase Function in Endosome and
931 Lysosome Biogenesis. Trends Cell Biol 28:957-970.
932 76. Bohdanowicz M, Balkin DM, De Camilli P, Grinstein S. 2012. Recruitment of OCRL
933 and Inpp5B to phagosomes by Rab5 and APPL1 depletes phosphoinositides and
934 attenuates Akt signaling. Mol Biol Cell 23:176-87.
935 77. Choudhury A, Dominguez M, Puri V, Sharma DK, Narita K, Wheatley CL, Marks DL,
936 Pagano RE. 2002. Rab proteins mediate Golgi transport of caveola-internalized
937 glycosphingolipids and correct lipid trafficking in Niemann-Pick C cells. J Clin Invest
938 109:1541-50.
939 78. Tebaldi G, Pritchard, S.M., Nicola, A.V. 2020. Herpes simplex virus entry by a non-
940 conventional endocytic pathway. J Virol doi:10.1128/JVI.01910-20.
941 79. Van Acker T, Tavernier J, Peelman F. 2019. The Small GTPase Arf6: An Overview of Its
942 Mechanisms of Action and of Its Role in Host(-)Pathogen Interactions and Innate
943 Immunity. Int J Mol Sci 20.
944 80. Garcia-Exposito L, Barroso-Gonzalez J, Puigdomenech I, Machado JD, Blanco J,
945 Valenzuela-Fernandez A. 2011. HIV-1 requires Arf6-mediated membrane dynamics to
946 efficiently enter and infect T lymphocytes. Mol Biol Cell 22:1148-66.
947 81. Heikkila O, Susi P, Tevaluoto T, Harma H, Marjomaki V, Hyypia T, Kiljunen S. 2010.
948 Internalization of coxsackievirus A9 is mediated by {beta}2-microglobulin, dynamin, and
949 Arf6 but not by caveolin-1 or clathrin. J Virol 84:3666-81.
950 82. Mercer J, Helenius A. 2008. Vaccinia virus uses macropinocytosis and apoptotic mimicry
951 to enter host cells. Science 320:531-5.
952 83. Yoo JH, Shi DS, Grossmann AH, Sorensen LK, Tong Z, Mleynek TM, Rogers A, Zhu
953 W, Richards JR, Winter JM, Zhu J, Dunn C, Bajji A, Shenderovich M, Mueller AL,
954 Woodman SE, Harbour JW, Thomas KR, Odelberg SJ, Ostanin K, Li DY. 2016. ARF6 Is
955 an Actionable Node that Orchestrates Oncogenic GNAQ Signaling in Uveal Melanoma.
956 Cancer Cell 29:889-904.
957 84. Jackson CL, Walch L, Verbavatz JM. 2016. Lipids and Their Trafficking: An Integral
958 Part of Cellular Organization. Dev Cell 39:139-153.
959 85. Musarrat F, Jambunathan N, Rider PJF, Chouljenko VN, Kousoulas KG. 2018. The
960 Amino Terminus of Herpes Simplex Virus 1 Glycoprotein K (gK) Is Required for gB
961 Binding to Akt, Release of Intracellular Calcium, and Fusion of the Viral Envelope with
962 Plasma Membranes. J Virol 92.
963 86. Foster TP, Rybachuk GV, Kousoulas KG. 2001. Glycoprotein K specified by herpes
964 simplex virus type 1 is expressed on virions as a Golgi complex-dependent glycosylated
965 species and functions in virion entry. J Virol 75:12431-8.
966 87. Tal-Singer R, Peng C, Ponce De Leon M, Abrams WR, Banfield BW, Tufaro F, Cohen
967 GH, Eisenberg RJ. 1995. Interaction of herpes simplex virus glycoprotein gC with
968 mammalian cell surface molecules. J Virol 69:4471-83.
969 88. Komala Sari T, Gianopulos KA, Weed DJ, Schneider SM, Pritchard SM, Nicola AV.
970 2020. Herpes Simplex Virus Glycoprotein C Regulates Low-pH Entry. mSphere 5.
971 89. Rahn E, Petermann P, Hsu MJ, Rixon FJ, Knebel-Morsdorf D. 2011. Entry pathways of
972 herpes simplex virus type 1 into human keratinocytes are dynamin- and cholesterol-
973 dependent. PLoS One 6:e25464.
974 90. Clement C, Tiwari V, Scanlan PM, Valyi-Nagy T, Yue BY, Shukla D. 2006. A novel role
975 for phagocytosis-like uptake in herpes simplex virus entry. J Cell Biol 174:1009-21.

976 91. Devadas D, Koithan T, Diestel R, Prank U, Sodeik B, Dohner K. 2014. Herpes simplex
977 virus internalization into epithelial cells requires Na+/H+ exchangers and p21-activated
978 kinases but neither clathrin- nor caveolin-mediated endocytosis. J Virol 88:13378-95.
979 92. Praena B, Bello-Morales R, Lopez-Guerrero JA. 2020. Hsv-1 Endocytic Entry into a
980 Human Oligodendrocytic Cell Line is Mediated by Clathrin and Dynamin but Not
981 Caveolin. Viruses 12.
982 93. Bid HK, Roberts RD, Manchanda PK, Houghton PJ. 2013. RAC1: an emerging
983 therapeutic option for targeting cancer angiogenesis and metastasis. Mol Cancer Ther
984 12:1925-34.
985 94. Fretz M, Jin J, Conibere R, Penning NA, Al-Taei S, Storm G, Futaki S, Takeuchi T,
986 Nakase I, Jones AT. 2006. Effects of Na+/H+ exchanger inhibitors on subcellular
987 localisation of endocytic organelles and intracellular dynamics of protein transduction
988 domains HIV-TAT peptide and octaarginine. J Control Release 116:247-54.
989 95. Gekle M, Drumm K, Mildenberger S, Freudinger R, Gassner B, Silbernagl S. 1999.
990 Inhibition of Na+-H+ exchange impairs receptor-mediated albumin endocytosis in renal
991 proximal tubule-derived epithelial cells from opossum. J Physiol 520 Pt 3:709-21.
992 96. Margiotta A, Bucci C. 2019. Coordination between Rac1 and Rab Proteins: Functional
993 Implications in Health and Disease. Cells 8.
994 97. Huotari J, Helenius A. 2011. Endosome maturation. EMBO J 30:3481-500.
995 98. Gianni T, Campadelli-Fiume G, Menotti L. 2004. Entry of herpes simplex virus mediated
996 by chimeric forms of nectin1 retargeted to endosomes or to lipid rafts occurs through
997 acidic endosomes. J Virol 78:12268-76.
998 99. Zhang J, Feng Y, Forgac M. 1994. Proton conduction and bafilomycin binding by the V0
999 domain of the coated vesicle V-ATPase. J Biol Chem 269:23518-23.
1000 100. Cheshenko N, Pierce C, Herold BC. 2018. Herpes simplex viruses activate phospholipid
1001 scramblase to redistribute phosphatidylserines and Akt to the outer leaflet of the plasma
1002 membrane and promote viral entry. PLoS Pathog 14:e1006766.
1003 101. Zheng K, Chen M, Xiang Y, Ma K, Jin F, Wang X, Wang X, Wang S, Wang Y. 2014.
1004 Inhibition of herpes simplex virus type 1 entry by chloride channel inhibitors tamoxifen
1005 and NPPB. Biochem Biophys Res Commun 446:990-6.
1006 102. Scott CC, Vacca F, Gruenberg J. 2014. Endosome maturation, transport and functions.
1007 Semin Cell Dev Biol 31:2-10.
1008 103. Krummenacher C, Baribaud I, Sanzo JF, Cohen GH, Eisenberg RJ. 2002. Effects of
1009 herpes simplex virus on structure and function of nectin-1/HveC. J Virol 76:2424-33.
1010 104. Stults AM, Smith GA. 2019. The Herpes Simplex Virus 1 Deamidase Enhances
1011 Propagation but Is Dispensable for Retrograde Axonal Transport into the Nervous
1012 System. J Virol 93.
1013 105. Marconi P, Manservigi R. 2014. Herpes simplex virus growth, preparation, and assay.
1014 Methods Mol Biol 1144:19-29.
1015 106. Dai X, Zhou ZH. 2014. Purification of Herpesvirus Virions and Capsids. Bio Protoc 4.
1016 107. Kim DS, Dastidar H, Zhang C, Zemp FJ, Lau K, Ernst M, Rakic A, Sikdar S, Rajwani J,
1017 Naumenko V, Balce DR, Ewanchuk BW, Tailor P, Yates RM, Jenne C, Gafuik C,
1018 Mahoney DJ. 2017. Smac mimetics and oncolytic viruses synergize in driving anticancer
1019 T-cell responses through complementary mechanisms. Nat Commun 8:344.
1020 108. Beug ST, Beauregard CE, Healy C, Sanda T, St-Jean M, Chabot J, Walker DE, Mohan A,
1021 Earl N, Lun X, Senger DL, Robbins SM, Staeheli P, Forsyth PA, Alain T, LaCasse EC,

1022 Korneluk RG. 2017. Smac mimetics synergize with immune checkpoint inhibitors to
1023 promote tumour immunity against glioblastoma. Nat Commun 8.
1024 109. Li L, Wan T, Wan M, Liu B, Cheng R, Zhang R. 2015. The effect of the size of
1025 fluorescent dextran on its endocytic pathway. Cell Biol Int 39:531-9.
1026 110. Schindelin J, Arganda-Carreras I, Frise E, Kaynig V, Longair M, Pietzsch T, Preibisch S,
1027 Rueden C, Saalfeld S, Schmid B, Tinevez JY, White DJ, Hartenstein V, Eliceiri K,
1028 Tomancak P, Cardona A. 2012. Fiji: an open-source platform for biological-image
1029 analysis. Nat Methods 9:676-82.
1030

1031 **Figure Legends**

1032 **Fig. 1. VSVΔG-BHLD pseudotype narrow cellular tropism is not due to differences in**

1033 **relative glycoprotein ratios or receptor expression levels.** HSV-1 (A) and VSVΔG-BHLD (B)

1034 entry was assessed on nine cell lines, B78H1, C10, CHO-K1, CHO-nectin-1, CHO-HVEM,

1035 HeLa, Vero, HaCaT, and SH-SY5Y. Cells were infected at a MOI of 1. Entry was quantitated by

1036 flow cytometry at 6 hours post infection. C) Cell surface expression of nectin-1 (C) and HVEM

1037 (D) was analyzed by flow cytometry. Surface levels of nectin-1 were quantitated by staining

1038 cells with an anti-nectin-1 monoclonal antibody CK41 conjugated to phycoerythrin (PE) (green

1039 histograms). Surface levels of HVEM were quantitated by staining cells with an anti-HVEM

1040 polyclonal antibody R140 and a FITC-labeled secondary antibody (cyan). Blue histograms are

1041 isotype controls. Red histograms are mock (no antibody) controls. E and F) Relative ratios of

1042 gB:gH:gL:gD for HSV-1 and VSVΔG-BHLD particles. HSV-1 and VSVΔG-BHLD virions

1043 were purified either through a continuous sucrose gradient (HSV-1) or continuous Optiprep

1044 gradient (VSVΔG-BHLD), pelleted, and analyzed for their glycoprotein content (gB, gH, gL,

1045 and gD) by western blot (anti-gB pAb R68, anti-gH pAb R137, anti-gL mAb L1, and anti-gD

1046 pAb R7). A representative western blot is shown. The amounts of gB, gH, gL, and gD in three

1047 different virion preparations were determined by densitometry. Levels of gH, gL, and gD were

1048 normalized to gB levels from their respective virions. A Student's T-test with Welch's correction

1049 was used to determine the significance of differences between relative amounts of gH, gL, or gD
1050 between HSV-1 and VSVΔG-BHLD virions (ns = not significant; $p < 0.05$ = *; $p < 0.01$ = **; p
1051 < 0.001 = ***).
1052
1053 **Fig. 2. HSV-1 and VSVΔG-BHLD enter cells by endocytosis.** C10 (A and B) and CHO-
1054 HVEM (C and D) cells were pretreated with a hypertonic solution of sucrose (0.3 M) and
1055 infected with HSV-1 and VSVΔG-BHLD at MOI = 1. Infectivity was quantitated by flow
1056 cytometry at 6 hours post infection. Significance was calculated using a two-tailed Student's T-
1057 test with Welch's correction ($p < 0.05$ = *; $p < 0.01$ = **; $p < 0.001$ = ***).
1058
1059 **Fig. 3. Both HSV-1 and VSVΔG-BHLD require dynamin but only HSV-1 requires clathrin**
1060 **for entry .** C10 (A and C) and CHO-HVEM (B and D) cells were pretreated with dynamin
1061 inhibitors Dynasore (80 μM), Dyngo-4a (25 μM), MiTMAB (5 μM), or the CME inhibitor,
1062 Pitstop-2 (30 μM) and infected with HSV-1 or VSVΔG-BHLD at MOI = 1. Infectivity was
1063 quantitated by flow cytometry at 6 hours post infection. CHO-HVEM cells treated with Dyngo-
1064 4a or MiTMAB used the same DMSO control, as indicated by the same bar graph appearing
1065 twice each in panels C and D. Significance was calculated using a two-tailed Student's T-test
1066 with Welch's correction ($p < 0.05$ = *; $p < 0.01$ = **; $p < 0.001$ = ***).
1067
1068 **Fig. 4. HSV-1 and VSVΔG-BHLD entry requires cellular cholesterol but not caveolin-1.**
1069 C10 (A and B) and CHO-HVEM (C and D) cells were pretreated with a cholesterol-removal
1070 drug methyl-β-cyclodextran, MβCD (5 mM) and infected with HSV-1 (A and C) or VSVΔG-
1071 BHLD (B and D) at MOI = 1. Infectivity was quantitated by flow cytometry at 6 hours post

1072 infection. E) CHO-HVEM cells were transfected with a caveolin-1 siRNA (cav-1) or a
1073 scrambled control siRNA (scr) (both 50 pm) and infected with HSV-1 or VSVΔG-BHLD at
1074 MOI = 1. Infectivity was quantitated by flow cytometry at 6 hours post infection. Significance
1075 was calculated using a two-tailed Student's T-test with Welch's correction ($p < 0.05$ = *; $p <$
1076 0.01 = **; $p < 0.001$ = ***). F) Western blot analyses, using antibody clone 4H312 (Santa Cruz
1077 Biotechnology), of caveolin-1 knockdown in CHO-HVEM cells (representative of three western
1078 blots, one from each biological replicate). G) Western blot analyses, using antibody clone 4H312
1079 (Santa Cruz Biotechnology), of caveolin-1 levels in C10, CHO-HVEM, and 3T12 cells.
1080
1081 **Fig. 5. Neither HSV-1 nor VSVΔG-BHLD entry requires macropinocytosis.** C10 (A and B)
1082 and CHO-HVEM (C and D) cells were pretreated with macropinocytosis inhibitors cytochalasin
1083 D (2 μM), EIPA (25 μM), or NSC23766 (200 μM) and infected with HSV-1 or VSVΔG-BHLD
1084 at MOI = 1. Infectivity was quantitated by flow cytometry at 6 hours post infection. Significance
1085 was calculated using a two-tailed Student's T-test with Welch's correction (ns = not significant;
1086 $p < 0.05$ = *; $p < 0.01$ = **; $p < 0.001$ = ***).
1087
1088 **Fig 6**: **Roles of Rabs 5 and 7 and Arf6 in HSV-1 and VSVΔG-BHLD entry.** The roles of the
1089 small GTPases Rab5, Rab7 (A, C, E, G), and Arf6 (B, D, F, H) were assessed for HSV-1 (A, B,
1090 E, F) and VSVΔG-BHLD (C, D, G, H) entry into C10 (A, B, C, D) and CHO-HVEM (E, F, G,
1091 H) cells. C10 (A and C) and CHO-HVEM (E and G) cells were transfected with either an empty
1092 vector control (eGFP or mCherry), eGFP or mCherry-tagged Rab5 dominant negative (DN), or
1093 eGFP or mCherry-tagged Rab7DN. Cells were infected at an MOI = 1 with either HSV-1 or
1094 VSVΔG-BHLD. Entry was assessed by flow cytometry at 6 hpi. The percent of infected cells

1095 was determined by dividing the number of virus(+)eGFP/mCherry(+) cells by the total number
1096 of eGFP/mCherry(+) cells. C10 (B and D) and CHO-HVEM cells (F and H) were treated with
1097 the Arf6 inhibitor NAV-2729 (25 μM) and infected with either HSV-1 or VSVΔG-BHLD at an
1098 MOI = 1. Significance was calculated using a two-tailed Student's T-test with Welch's
1099 correction (ns = not significant; $p < 0.05$ = *; $p < 0.01$ = **; $p < 0.001$ = ***).
1100
1101 **Fig. 7. VSVΔG-BHLD entry requires endosomal acidification in a cell-dependent manner.**
1102 C10 (A and B) and CHO-HVEM (C and D) cells were pretreated with inhibitors of endosomal
1103 acidification BFLA (100 nM), NH_4Cl (50 mM), or monensin (15 μM) and infected with HSV-1
1104 or VSVΔG-BHLD at MOI = 1. Infectivity was quantitated by flow cytometry at 6 hours post
1105 infection. Significance was calculated using a two-tailed Student's T-test with Welch's
1106 correction ($p < 0.05$ = *; $p < 0.01$ = **; $p < 0.001$ = ***).
1107
1108 **Fig. 8. gC increases entry efficiency into CHO-HVEM and HaCaT cells.** A) Incorporation of
1109 gC was verified by western blot of pelleted and washed virions. B) VSVΔG-BHLD-pCAGGS
1110 and VSVΔG-BHLD-C entry was assessed on nine cell lines, B78H1, C10, CHO-K1, CHO-
1111 nectin-1, CHO-HVEM, HeLa, Vero, HaCaT, and SH-SY5Y. Cells were infected at a MOI of 1.
1112 Entry was quantitated by flow cytometry at 6 hours post infection. Significance was calculated
1113 using a two-tailed Student's T-test with Welch's correction ($p < 0.05$ = *; $p < 0.01$ = **; $p <$
1114 0.001 = ***).
1115
1116 **Fig. 9. Entry model of VSVΔG-BHLD and HSV-1.** A) Entry of VSVΔG-BHLD and HSV-1
1117 entry into C10 and CHO-HVEM cells occurs by endocytosis and requires dynamin and

1118 cholesterol. VSVΔG-BHLD entry into C10 and CHO-HVEM cells additionally requires NHE
1119 and Rac1 activity whereas HSV-1 does not. VSVΔG-BHLD entry into C10 cells, but not CHO-
1120 HVEM cells also requires Rab5 and endosomal acidification. HSV-1 does not require either
1121 Rab5 or endosomal acidification for entry into either cell type. B) Table summarizing the cellular
1122 molecules important for HSV-1 and VSVΔG-BHLD entry into C10 and CHO-HVEM cells.
1123 Green check marks indicate that the virus requires that cellular component for entry. Red X-
1124 marks indicate that the virus does not require that cellular component for entry.
1125

1126 **Supplemental Figure Legends**

1127 **Fig. S1. Infecting cells with VSVΔG-BHLD at a higher MOI does not increase entry to an**
1128 **appreciable extent.** A)Receptor null (B78H1 and CHO-K1) and receptor bearing cells (C10,
1129 CHO-HVEM, HeLa, Vero, HaCaT, and SH-SY5Y) were infected at MOI =1 (red) or MOI = 10
1130 (purple). Entry efficiency was assessed by flow cytometry at 6 hours post infection. B and C)
1131 Receptor null (B78H1 and CHO-K1) and receptor bearing cells (C10, CHO-HVEM, HeLa, Vero,
1132 HaCaT, and SH-SY5Y) were infected at MOI =1 with either VSVΔG-G (B) or VSVΔG-PIV5
1133 (C). Entry was assessed by flow cytometry at 6 hours post infection.
1134

1135 **Fig. S2. VSVΔG-G and VSVΔG-PIV5 entry in the presence of hypertonic sucrose.** C10 (A,
1136 B) and CHO-HVEM (C, D) cells were pretreated with a hypertonic solution of sucrose (0.3 M)
1137 and infected with VSVΔG-G or VSVΔG-PIV5 at MOI = 1. Infectivity was quantitated by flow
1138 cytometry at 6 hours post infection. Significance was calculated using a two-tailed Student's T-
1139 test with Welch's correction ($p < 0.05$ = *; $p < 0.01$ = **; $p < 0.001$ = ***). E) C10 and CHO-
1140 HVEM cells were pretreated with 0.3 M sucrose and incubated with 50 ug/ml of AF488-labeled

1141 transferrin (Tf). Cells were fixed, counterstained with DAPI, and imaged by confocal

1142 microscopy. Scale bar = 25 μm.

1143

1144 **Fig. S3 VSVΔG-G and VSVΔG-PIV5 differ in their dependence on dynamin and clathrin**

1145 **for entry.** C10 (A and C) and CHO-HVEM (B and D) cells were pretreated with dynamin

1146 inhibitors Dynasore (80 μM), Dyngo-4a (25 μM), MiTMAB (5 μM), or the CME inhibitor

1147 Pitstop-2 (30 μM) and infected with VSVΔG-G or VSVΔG-PIV5 at a MOI of 1. Infectivity was

1148 quantitated by flow cytometry at 6 hours post infection. CHO-HVEM cells treated with Dyngo-

1149 4a or MiTMAB used the same DMSO control as indicated by the same bar graph appearing

1150 twice each in panels C and D. Significance was calculated using a two-tailed Student's T-test

1151 with Welch's correction ($p < 0.05$ = *; $p < 0.01$ = **; $p < 0.001$ = ***). E and F) C10 and CHO-

1152 HVEM cells were pretreated with dynamin inhibitors Dynasore, Dyngo-4a, MiTMAB, or

1153 Pitstop-2 at the same concentrations as in panels A-D and then incubated with 50 μg/ml of

1154 AF488-labeled transferrin. Cells were fixed, counterstained with DAPI, and imaged by confocal

1155 microscopy. Scale bar = 25 μm.

1156

1157 **Fig. S4. VSVΔG-G entry does not require cholesterol whereas VSVΔG-PIV5 entry**

1158 **requires cholesterol in a cell-type-dependent manner.** C10 (A and B) and CHO-HVEM (C

1159 and D) cells were pretreated with a cholesterol-removal drug methyl-β-cyclodextran, MβCD (5

1160 mM) and infected with VSVΔG-G or VSVΔG-PIV5 at a MOI of 1. Infectivity was quantitated

1161 by flow cytometry at 6 hours post infection. E) C10 and CHO-HVEM cells were treated with

1162 either a solvent control (H_2O/EtOH) or methyl-β-cyclodextrin (MβCD), then incubated with

1163 cholera toxin subunit B labelled with Alexa Fluor 488. Confocal microscopy was performed on

1164 the solvent control and methyl-β-cyclodextrin treated cells. Cells were fixed, counterstained with
1165 DAPI, and imaged by confocal microscopy. Scale bar = 25 μm. (F) CHO-HVEM cells were
1166 transfected with a caveolin-1 siRNA (cav-1) or a scrambled control siRNA (scr) (both 50 pm)
1167 and infected with VSVΔG-G or VSVΔG-PIV5 at a MOI of 1. Infectivity was quantitated by
1168 flow cytometry at 6 hours post infection. Significance was calculated using a two-tailed
1169 Student's T-test with Welch's correction ($p < 0.05$ = *; $p < 0.01$ = **; $p < 0.001$ = ***).
1170
1171 **Fig. S5. VSVΔG-BHLD does not co-localize with the fluid-phase marker 70 kDa dextran in**
1172 **C10 cells.** C10 cells were incubated with 1 mg/ml of rhodamine-B labelled 70 kDa dextran and
1173 VSVΔG-BHLD (MOI = 1) for one hour at 4° C. Cells were then shifted to 37° C for 20 minutes.
1174 Cells were fixed, counterstained with DAPI, and imaged by confocal microscopy. gB was
1175 detected by immunofluorescence using the rabbit pAb R68 and anti-rabbit IgG conjugated to
1176 FITC. Green = gB (marker for VSVΔG-BHLD particles); Red = 70 kDa dextran. Scale bar = 25
1177 μm.
1178
1179 **Fig. S6. VSVΔG-BHLD, in large, does not co-localized with the fluid-phase marker, 70 kDa**
1180 **dextran, in CHO-HVEM cells.** CHO-HVEM cells were incubated with 1 mg/ml of rhodamine-
1181 B labelled 70 kDa dextran and VSVΔG-BHLD (MOI = 1) for one hour at 4°C. Cells were then
1182 shifted to 37° C for 20 minutes. Cells were fixed, counterstained with DAPI, and imaged by
1183 confocal microscopy. gB was detected by immunofluorescence using the rabbit pAb R68 and
1184 anti-rabbit IgG conjugated to FITC. Green = gB (marker for VSVΔG-BHLD particles); Red = 70
1185 kDa dextran. Scale bar = 25 μm.
1186

1187 **Fig. S7. VSVΔG-G and VSVΔG-PIV5 entry does not require macropinocytosis.** C10 (A and
1188 B) and CHO-HVEM (C and D) cells were pretreated with macropinocytosis inhibitors
1189 cytochalasin D (2 μM), EIPA (25 μM), or NSC23766 (200 μM) and infected with VSVΔG-G or
1190 VSVΔG-PIV5 at a MOI of 1. Infectivity was quantitated by flow cytometry at 6 hours post
1191 infection. Significance was calculated using a two-tailed Student's T-test with Welch's
1192 correction ($p < 0.05$ = *; $p < 0.01$ = **; $p < 0.001$ = ***). E) C10 and CHO-HVEM cells were
1193 pretreated with macropinocytosis inhibitors cytochalasin D, EIPA, or NSC23766 at the same
1194 concentrations as in panels A-D and then incubated with 1.0 mg/ml of Rhodamine-B-labeled 70-
1195 kDa dextran (Dex). Cells were fixed, counterstained with DAPI, and imaged by confocal
1196 microscopy. Scale bar = 25 μm.
1197
1198 **Fig. S8**: **Roles of Rab5, Rab7, and Arf6 in VSVΔG-G and VSVΔG-PIV5 entry.** The roles of
1199 the small GTPases Rab5, Rab7 (A, C, E, G), and Arf6 (B, D, F, H) were assessed for VSVΔG-G
1200 (A, B, E, F) and VSVΔG-PIV5 (C, D, G, H) entry into C10 (A, B, C, D) and CHO-HVEM (E, F,
1201 G, H) cells. C10 (A and C) and CHO-HVEM (E and G) cells were transfected with either an
1202 empty vector control (eGFP or mCherry), eGFP or mCherry-tagged Rab5 dominant negative
1203 (DN), or eGFP or mCherry-tagged Rab7DN. Cells were infected at an MOI = 1 with either
1204 VSVΔG-G or VSVΔG-PIV5. Entry was assessed by flow cytometry at 6 hpi. The percent of
1205 infected cells was determined by dividing the number of virus(+)/eGFP/mCherry(+) cells by the
1206 total number of eGFP/mCherry(+) cells. C10 (B and D) and CHO-HVEM cells (F and H) were
1207 treated with the Arf6 inhibitor NAV-2729 (25 μM) and infected with either VSVΔG-G or
1208 VSVΔG-PIV5 at an MOI = 1. Significance was calculated using a two-tailed Student's T-test
1209 with Welch's correction (ns = not significant; $p < 0.05$ = *; $p < 0.01$ = **; $p < 0.001$ = ***).

1210

1211 **Fig. S9. VSVΔG-G but not VSVΔG-PIV5 entry requires endosomal acidification.** C10 (A

1212 and B) and CHO-HVEM (C and D) cells were pretreated with inhibitors of endosomal

1213 acidification BFLA (100 nM), NH_4Cl (50 mM), or monensin (15 μM) and infected with

1214 VSVΔG-G or VSVΔG-PIV5 at MOI = 1. Infectivity was quantitated by flow cytometry at 6

1215 hours post infection. Significance was calculated using a two-tailed Student's T-test with

1216 Welch's correction ($p < 0.05$ = *; $p < 0.01$ = **; $p < 0.001$ = ***). E) C10 and CHO-HVEM

1217 cells were pretreated with inhibitors of endosomal acidification at the same concentrations as in

1218 panels A-D (BFLA, NH_4Cl, or monensin) and then incubated with Lysotracker (1 μM). Cells

1219 were fixed, counterstained with DAPI, and imaged by confocal microscopy. Scale bar = 25 μm.

1220

1221 **Table S1. Sensitivity of HSV-1, VSVΔG-BHLD, VSVΔG-G, and VSVΔG-PIV5 to specific**

1222 **inhibitors.** Green check marks indicate that virus entry is sensitive to that particular inhibitor.

1223 Red X marks indicate that the virus is not sensitive to that particular inhibitor.

1224

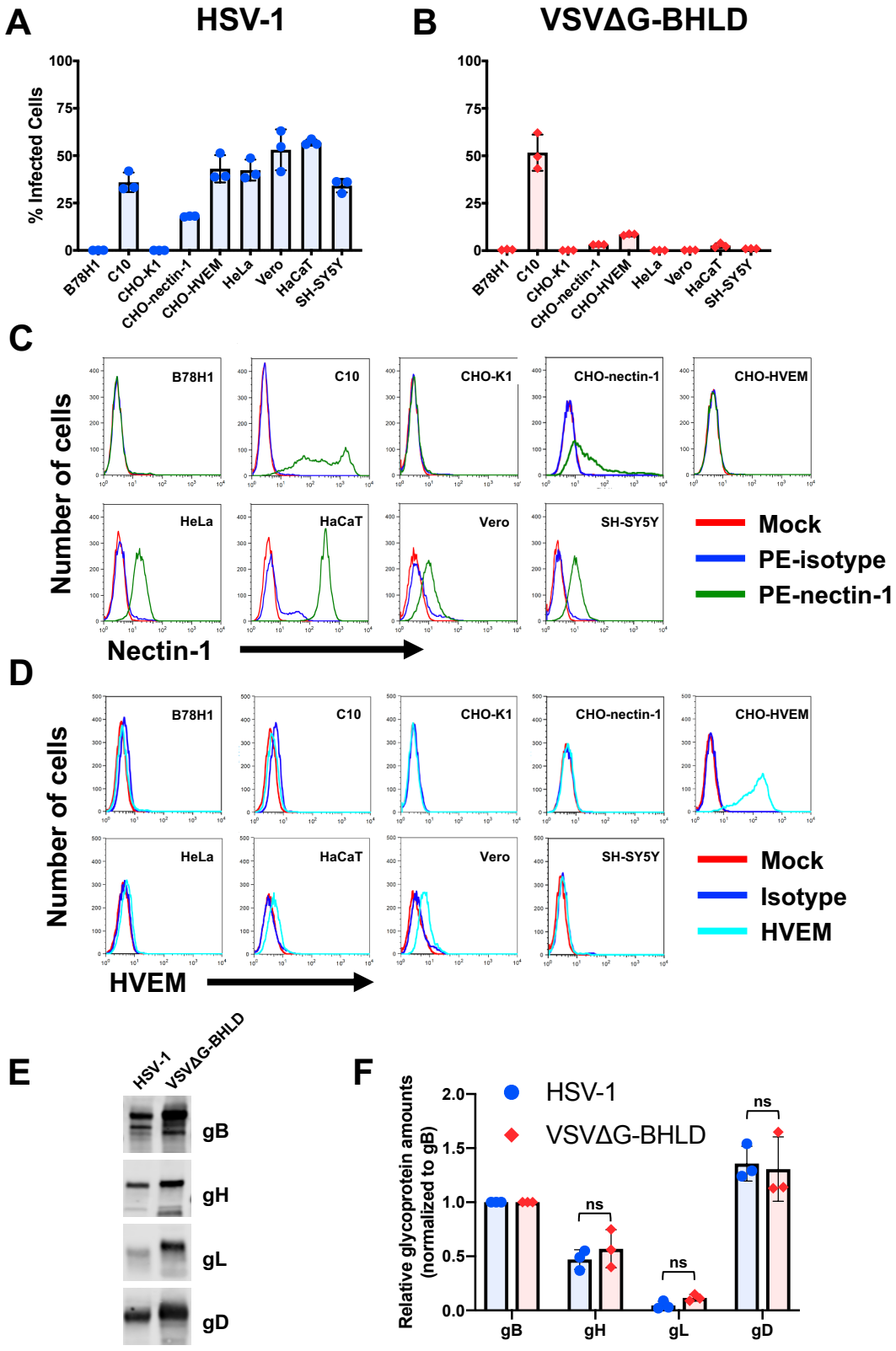
A
HSV-1
% Infected Cells
100
75
50
25
0
B78H1
C10
CHO-K1
CHO-nectin-1
CHO-HVEM
HeLa
Vero
HaCaT
SH-SY5Y
B
VSVΔG-BHLD
C
Number of cells
Nectin-1
Mock
PE-isotype
PE-nectin-1
D
HVEM
Isotype
E
HSV-1
VSVΔG-BHLD
gB
gH
gL
gD
F
Relative glycoprotein amounts (normalized to gB)
2.0
1.5
1.0
0.5
0.0
ns

Fig. 1. VSVΔG-BHLD pseudotype narrow cellular tropism is not due to differences in relative glycoprotein ratios or receptor expression levels. HSV-1 (A) and VSVΔG-BHLD (B) entry was assessed on nine cell lines, B78H1, C10, CHO-K1, CHO-nectin-1, CHO-HVEM, HeLa, Vero, HaCaT, and SH-SY5Y. Cells were infected at a MOI of 1. Entry was quantitated by flow cytometry at 6 hours post infection. C) Cell surface expression of nectin-1 (C) and HVEM (D) was analyzed by flow cytometry. Surface levels of nectin-1 were quantitated by staining cells with an anti-nectin-1 monoclonal antibody CK41 conjugated to phycoerythrin (PE) (green histograms). Surface levels of HVEM were quantitated by staining cells with an anti-HVEM polyclonal antibody R140 and a FITC-labeled secondary antibody (cyan). Blue histograms are isotype controls. Red histograms are mock (no antibody) controls. E&F) Relative ratios of gB:gH:gL:gD for HSV-1 and VSVΔG-BHLD particles. HSV-1 and VSVΔG-BHLD virions were purified either through a continuous sucrose gradient (HSV-1) or continuous Optiprep gradient (VSVΔG-BHLD), pelleted, and analyzed for their glycoprotein content (gB, gH, gL, and gD) by Western blot (anti-gB pAb R68, anti-gH pAb = R137, anti-gL mAb L1, and anti-gD pAb R7). A representative Western blot is shown. The amounts of gB, gH, gL, and gD in three different virion preparations were determined by densitometry. Levels of gH, gL, and gD were normalized to gB levels from their respective virions. A Student's T-test with Welch's correction was used to determine the significance of differences between relative amounts of gH, gL, or gD between HSV-1 and VSVΔG-BHLD virions (ns = not significant; $p < 0.05$ = *; $p < 0.01$ = **; $p < 0.001$ = ***).

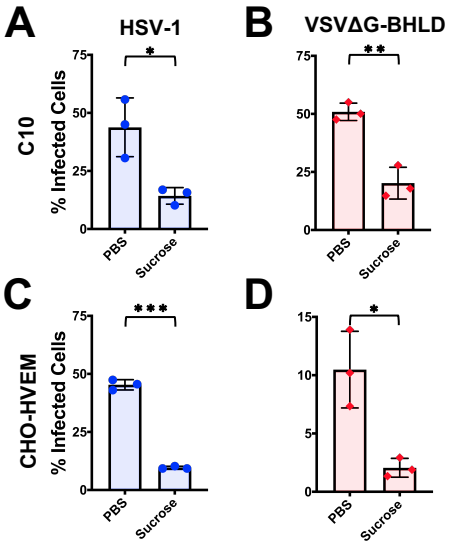

Fig. 2. HSV-1 and VSVΔG-BHLD enter cells by endocytosis. C10 (A and B) and CHO-HVEM (C and D) cells were pretreated with a hypertonic solution of sucrose (0.3 M) and infected with HSV-1 and VSVΔG-BHLD at MOI = 1. Infectivity was quantitated by flow cytometry at 6 hours post infection. Significance was calculated using a two-tailed Student's T-test with Welch's correction ($p < 0.05$ = *; $p < 0.01$ = **; $p < 0.001$ = ***).

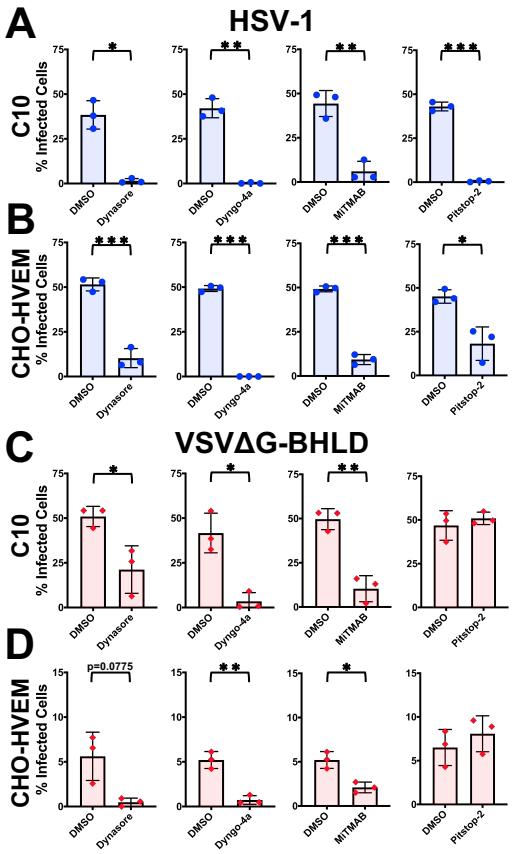

Fig. 3. Both HSV-1 and VSVΔG-BHLD require dynamin but only HSV-1 requires clathrin for entry . C10 (A and C) and CHO-HVEM (B and D) cells were pretreated with dynamin inhibitors Dynasore (80 μM), Dyngo-4a (25 μM), MiTMAB (5 μM), or the CME inhibitor, Pitstop-2 (30 μM) and infected with HSV-1 or VSVΔG-BHLD at MOI = 1. Infectivity was quantitated by flow cytometry at 6 hours post infection. CHO-HVEM cells treated with Dyngo-4a or MiTMAB used the same DMSO control, as indicated by the same bar graph appearing twice each in panels C and D. Significance was calculated using a two-tailed Student's T-test with Welch's correction ($p < 0.05$ = *; $p < 0.01$ = **; $p < 0.001$ = ***).

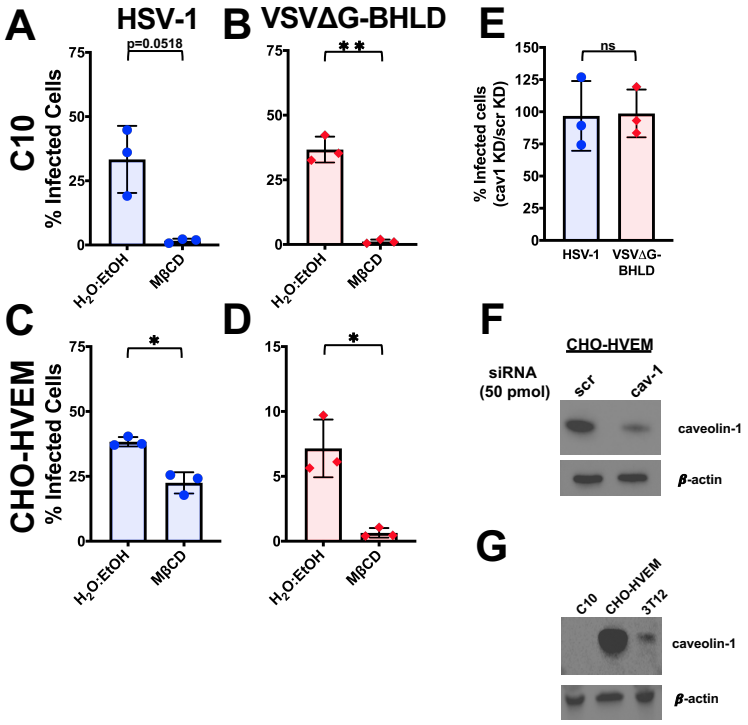

Fig. 4. HSV-1 and VSVΔG-BHLD entry requires cellular cholesterol but not caveolin-1. C10 (A and B) and CHO-HVEM (C and D) cells were pretreated with a cholesterol-removal drug methyl-β-cyclodextran, MβCD (5 mM) and infected with HSV-1 (A and C) or VSVΔG-BHLD (B and D) at MOI = 1. Infectivity was quantitated by flow cytometry at 6 hours post infection. E) CHO-HVEM cells were transfected with a caveolin-1 siRNA (cav-1) or a scrambled control siRNA (scr) (both 50 pm) and infected with HSV-1 or VSVΔG-BHLD at MOI = 1. Infectivity was quantitated by flow cytometry at 6 hours post infection. Significance was calculated using a two-tailed Student's T-test with Welch's correction ($p < 0.05$ = *; $p < 0.01$ = **; $p < 0.001$ = ***). F) Western blot analyses, using antibody clone 4H312 (Santa Cruz Biotechnology), of caveolin-1 knockdown in CHO-HVEM cells (representative of three western blots, one from each biological replicate). G) Western blot analyses, using antibody clone 4H312 (Santa Cruz Biotechnology), of caveolin-1 levels in C10, CHO-HVEM, and 3T12 cells.

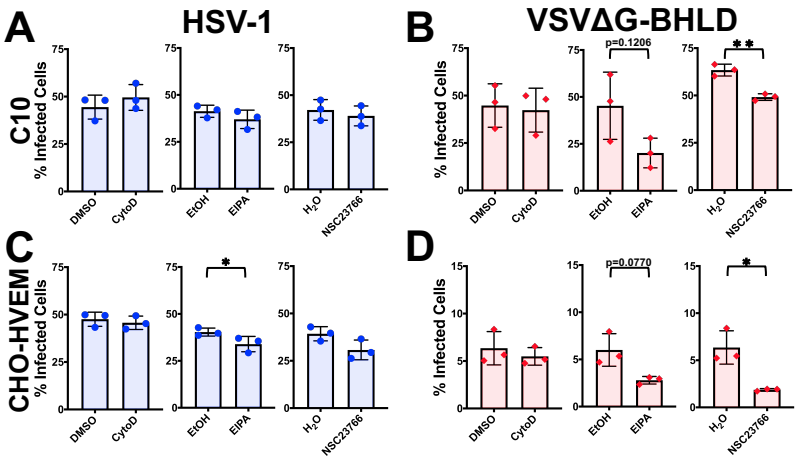

Fig. 5. Neither HSV-1 nor VSVΔG-BHLD entry requires macropinocytosis. C10 (A and B) and CHO-HVEM (C and D) cells were pretreated with macropinocytosis inhibitors cytochalasin D (2 μM), EIPA (25 μM), or NSC23766 (200 μM) and infected with HSV-1 or VSVΔG-BHLD at MOI = 1. Infectivity was quantitated by flow cytometry at 6 hours post infection. Significance was calculated using a two-tailed Student's T-test with Welch's correction (ns = not significant; $p < 0.05$ = *; $p < 0.01$ = **; $p < 0.001$ = ***).

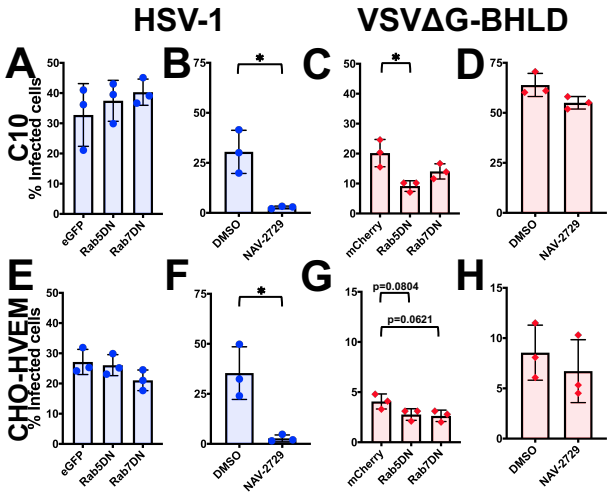

Fig 6: **Roles of Rabs 5 and 7 and Arf6 in HSV-1 and VSVΔG-BHLD entry.** The roles of the small GTPases Rab5, Rab7 (A, C, E, G), and Arf6 (B, D, F, H) were assessed for HSV-1 (A, B, E, F) and VSVΔG-BHLD (C, D, G, H) entry into C10 (A, B, C, D) and CHO-HVEM (E, F, G, H) cells. C10 (A and C) and CHO-HVEM (E and G) cells were transfected with either an empty vector control (eGFP or mCherry), eGFP or mCherry-tagged Rab5 dominant negative (DN), or eGFP or mCherry-tagged Rab7DN. Cells were infected at an MOI = 1 with either HSV-1 or VSVΔG-BHLD. Entry was assessed by flow cytometry at 6 hpi. The percent of infected cells was determined by dividing the number of virus(+)eGFP/mCherry(+) cells by the total number of eGFP/mCherry(+) cells. C10 (B and D) and CHO-HVEM cells (F and H) were treated with the Arf6 inhibitor NAV-2729 (25 μM) and infected with either HSV-1 or VSVΔG-BHLD at an MOI = 1. Significance was calculated using a two-tailed Student's T-test with Welch's correction (ns = not significant; $p < 0.05$ = *; $p < 0.01$ = **; $p < 0.001$ = ***).

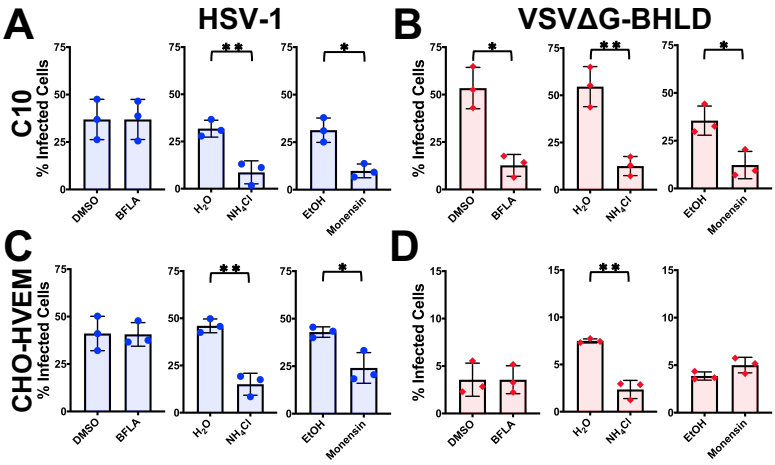

Fig. 7. VSVΔG-BHLD entry requires endosomal acidification in a cell-dependent manner. C10 (A and B) and CHO-HVEM (C and D) cells were pretreated with inhibitors of endosomal acidification BFLA (100 nM), NH_4Cl (50 mM), or monensin (15 μM) and infected with HSV-1 or VSVΔG-BHLD at MOI = 1. Infectivity was quantitated by flow cytometry at 6 hours post infection. Significance was calculated using a two-tailed Student's T-test with Welch's correction ($p < 0.05$ = *; $p < 0.01$ = **; $p < 0.001$ = ***).

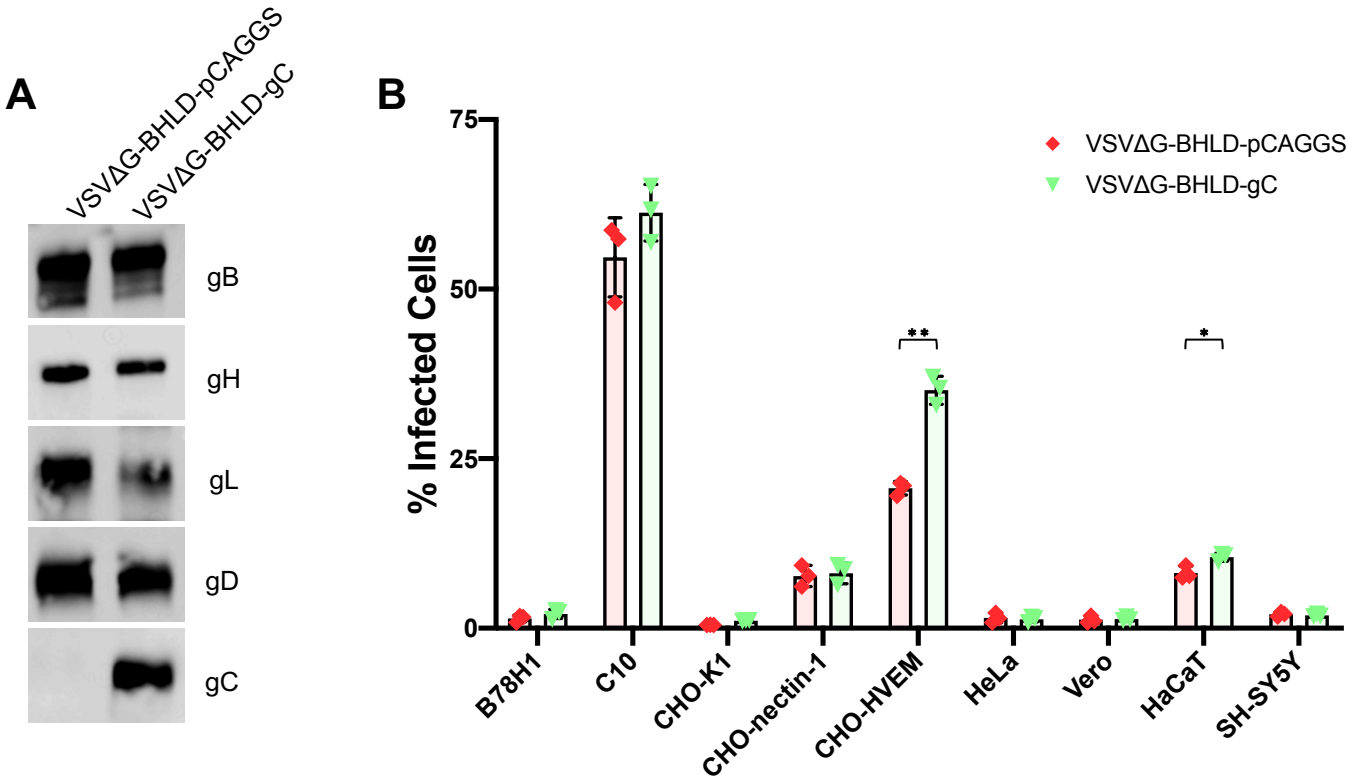

Fig. 8. gC increases entry efficiency into CHO-HVEM and HaCaT cells. A) Incorporation of gC was verified by western blot of pelleted and washed virions. B) VSVΔG-BHLD-pCAGGS and VSVΔG-BHLD-gC entry was assessed on nine cell lines, B78H1, C10, CHO-K1, CHO-nectin-1, CHO-HVEM, HeLa, Vero, HaCaT, and SH-SY5Y. Cells were infected at a MOI of 1. Entry was quantitated by flow cytometry at 6 hours post infection. Significance was calculated using a two-tailed Student's T-test with Welch's correction ($p < 0.05$ = *; $p < 0.01$ = **; $p < 0.001$ = ***).

A

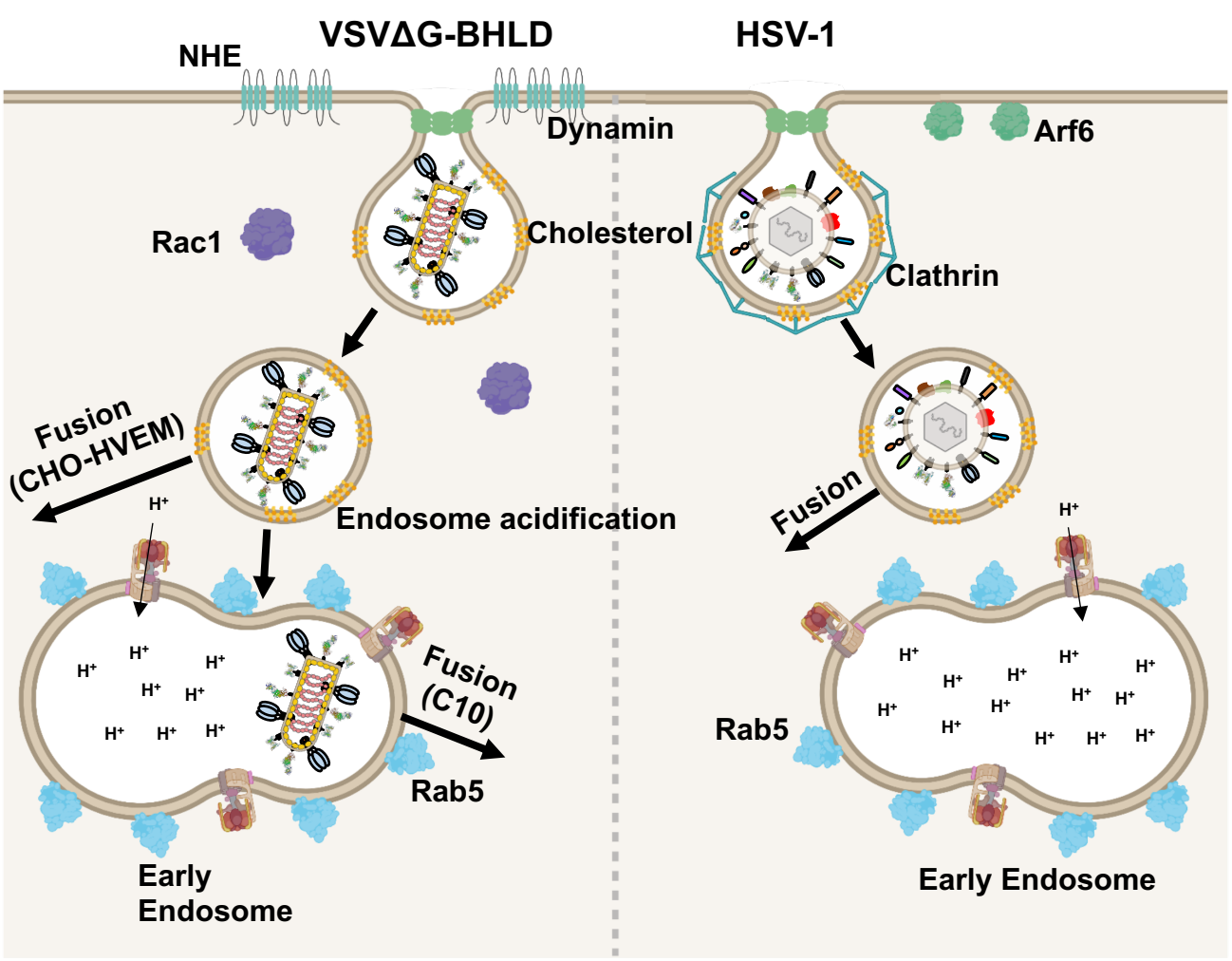

B

		Endocytosis	Dynamin	Clathrin	Cholesterol	Caveolin	Macropino -cytosis	Small GTPases	Low pH
C10	HSV-1	✓	✓	✓	✓	X	X	Arf6 ✓ Rab5/7 X	X
C10	VSVΔG-BHLD	✓	✓	X	✓	X	X	Arf6 X Rab5/7 ✓	✓
CHO-HVEM	HSV-1	✓	✓	✓	✓	X	X	Arf6 ✓ Rab5/7 X	X
CHO-HVEM	VSVΔG-BHLD	✓	✓	X	✓	X	X	Arf6 X Rab5/7 X	X

Fig. 9. Entry model of VSVΔG-BHLD and HSV-1. A) Entry of VSVΔG-BHLD and HSV-1 entry into C10 and CHO-HVEM cells occurs by endocytosis and requires dynamin and cholesterol. VSVΔG-BHLD entry into C10 and CHO-HVEM cells additionally requires NHE and Rac1 activity whereas HSV-1 does not. VSVΔG-BHLD entry into C10 cells, but not CHO-HVEM cells also requires Rab5 and endosomal acidification. HSV-1 does not require either Rab5 or endosomal acidification for entry into either cell type. B) Table summarizing the cellular molecules important for HSV-1 and VSVΔG-BHLD entry into C10 and CHO-HVEM cells. Green check marks indicate that the virus requires that cellular component for entry. Red X marks indicate that the virus does not require that cellular component for entry.